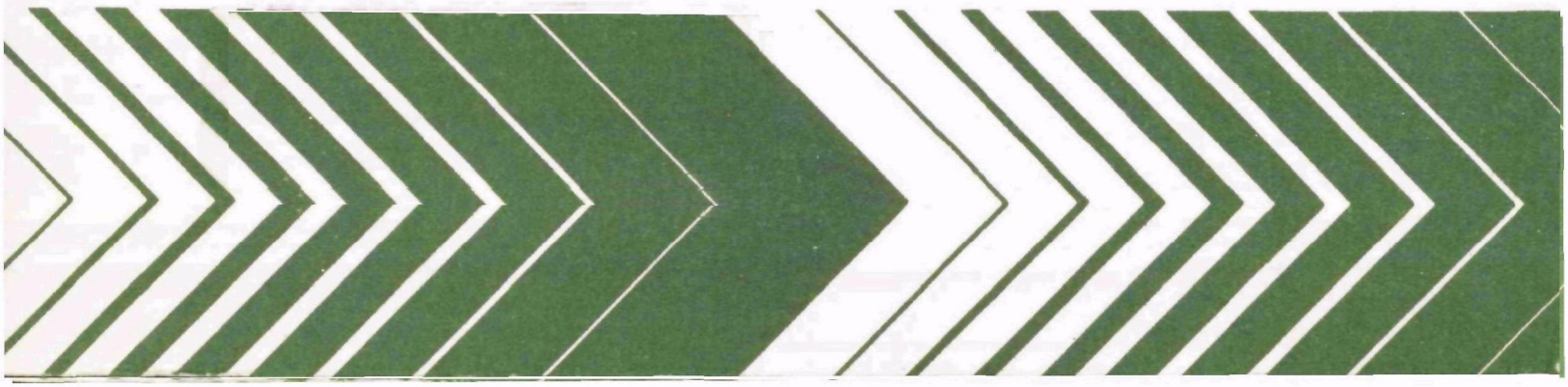


Research and Development



# Investigation of Particulate Matter Monitoring Using Contact Electricity

## Final Report



## **RESEARCH REPORTING SERIES**

Research reports of the Office of Research and Development, U S. Environmental Protection Agency, have been grouped into nine series. These nine broad categories were established to facilitate further development and application of environmental technology. Elimination of traditional grouping was consciously planned to foster technology transfer and a maximum interface in related fields. The nine series are:

1. Environmental Health Effects Research
2. Environmental Protection Technology
3. Ecological Research
4. Environmental Monitoring
5. Socioeconomic Environmental Studies
6. Scientific and Technical Assessment Reports (STAR)
7. Interagency Energy-Environment Research and Development
8. "Special" Reports
9. Miscellaneous Reports

This report has been assigned to the ENVIRONMENTAL PROTECTION TECHNOLOGY series. This series describes research performed to develop and demonstrate instrumentation, equipment, and methodology to repair or prevent environmental degradation from point and non-point sources of pollution. This work provides the new or improved technology required for the control and treatment of pollution sources to meet environmental quality standards.

This document is available to the public through the National Technical Information Service, Springfield, Virginia 22161.

EPA-600/2-78-212  
October 1978

INVESTIGATION OF PARTICULATE MATTER MONITORING  
USING CONTACT ELECTRICITY

Final Report

by

Walter John, Georg Reischl, William Devor  
and Jerome J. Wesolowski

Air and Industrial Hygiene Laboratory Section  
California Department of Health Services  
Berkeley, California 94704

Grant Number R 803719-01-2

Project Officer

John Nader  
Emissions Measurements and Characterization Division  
Environmental Sciences Research Laboratory  
Research Triangle Park, North Carolina 27711

ENVIRONMENTAL SCIENCES RESEARCH LABORATORY  
OFFICE OF RESEARCH AND DEVELOPMENT  
U.S. ENVIRONMENTAL PROTECTION AGENCY  
RESEARCH TRIANGLE PARK, NORTH CAROLINA 27711

# DISCLAIMER

This report has been reviewed by the Environmental Sciences Research Laboratory, U.S. Environmental Protection Agency, and approved for publication. Approval does not signify that the contents necessarily reflect the views and policies of the U.S. Environmental Protection Agency, nor does mention of trade names or commercial products constitute endorsement or recommendation for use.

## ABSTRACT

To better understand the contact electrification monitor for particulate matter, charge transfer by aerosol particles impacting on metal surfaces has been investigated. Monodisperse, uniformly charged or neutral aerosol particles (1-5  $\mu\text{m}$  diameter) from a vibrating orifice or fluidized bed generator were bounced on a metal probe. The transfer of precharge from the particles was found to be a sensitive indicator of the probe surface condition. A surface preparation procedure was developed which yielded linear charge transfer curves.

Measurements were made of methylene blue, potassium biphthalate, sodium chloride and aluminum particles impacting on stainless steel, Inconel, titanium and platinum probes. For insulating materials, the transfer of precharge was independent of particle size while the contact charge was proportional to the cube of particle diameter and directly proportional to impact velocity. The magnitude of the contact charge was strongly dependent on the electrical resistivity of the material. A theoretical model was found to account semi-quantitatively for all aspects of the data. A major remaining difficulty is the lack of knowledge of the contact potential. The implications of these findings for monitoring applications is discussed in detail and the advantages and disadvantages of the monitor are assessed.

## CONTENTS

Abstract.....	iii
Figures.....	vi
Tables.....	viii
Acknowledgments.....	ix
1. Introduction.....	1
2. Conclusions and Recommendations.....	3
3. Tests of the IKOR Monitor.....	4
Experimental Method.....	4
Results.....	4
4. Charge Transfer Experiments.....	8
Experimental Procedures.....	8
Measurements.....	17
5. Experiments with a Fluidized Bed Aerosol Generator.....	45
The Fluidized Bed.....	45
Charge Transfer Measurements with Aluminum Aerosol.....	52
6. Theory of Charge Transfer.....	58
Model of Charge Transfer Process.....	58
Discussion of the Theory.....	64
7. Implications of the Findings for Applications.....	65
Principal Factors Affecting Monitoring.....	65
Recommendations for Monitoring Procedures.....	66
Overall Assessment of the Contact Electrification Monitor.....	67
References.....	68

## FIGURES

<u>Number</u>		<u>Page</u>
1	Experimental Arrangement Used for Testing the IKOR Monitor.....	5
2	Experimental Arrangement for Charge Transfer Measurements.....	9
3	Apparatus for Induction Charging of Particles.....	10
4	Detail of the Area Where the Droplets are Formed.....	10
5	Typical Calibration Curve for the Particle Charger.....	11
6	Faraday Cup.....	13
7	Impaction Probe for Charge Transfer Measurements.....	15
8	Charge Transfer Curve Showing Surface Cleaning Effect.....	18
9	Nonlinear Charge Transfer Curve.....	20
10	Nonlinear Charge Transfer Curves.....	21
11	Linear Charge Transfer Curve Obtained with Polished Probe.....	23
12	Charge Transfer for Potassium Biphthalate Particles on Polished Stainless Steel.....	24
13	Contact Charge vs. Particle Diameter for Methylene Blue on Stainless Steel.....	25
14	Contact Charge vs. Particle Diameter for Sodium Chloride.....	26
15	Contact Charge vs. Particle Diameter for Potassium Biphthalate....	28
16	Contact Charge vs. Particle Diameter for Methylene Blue on Titanium.....	29
17	Contact Charge vs. Particle Velocity for Methylene Blue on Stainless Steel.....	31
18	Contact Charge/Mass for Various Materials.....	34
19	Charge Transfer for Potassium Biphthalate on Titanium.....	35

<u>Number</u>		<u>Page</u>
20	Charge Transfer for Potassium Biphthalate on Inconel.....	36
21	Charge Transfer for Sodium Chloride on Titanium.....	37
22	Charge Transfer for Sodium Chloride on Platinum.....	38
23	Time Dependence of Charge Transfer from Sodium Chloride on Titanium.....	39
24	Same as Figure 23 with Different Prior Probe Treatment.....	40
25	Time Dependence of Charge Transfer from Sodium Chloride on Platinum.....	41
26	Same as Figure 25 with Different Prior Probe Treatment.....	42
27	Fluidized Bed Aerosol Generator.....	45
28	Pressure Drop Across Fluidized Bed.....	46
29	Size Distribution of Aluminum Oxide Particles from the Fluidized Bed.....	48
30	Size Distribution of Aluminum Powder Sample.....	49
31	Concentration vs. Time of Aluminum Aerosol.....	50
32	Size Distribution of Aluminum Aerosol.....	51
33	Contact Charge and Particle Diameter vs. Time for Aluminum Aerosol.....	51
34	Charge Transferred from Aluminum Particles vs. Induction Voltage...	54
35	Contact Charge vs. Time After Restart.....	55
36	Slope of Charge Transfer Curve vs. Time.....	55
37	Data from Second Sample of Aluminum.....	56
38	Contact Charge of Aluminum vs. Velocity.....	57
39	Contact of Elastic Sphere with Surface During Impact.....	59



## TABLES

<u>Number</u>		<u>Page</u>
1	Contact Charge for Sodium Chloride Particles Impacting at 71 m/s on a Stainless Steel Probe.....	22
2	Charge Transfer Data for Methylene Blue Particles Impacting at 71 m/s on a Stainless Steel Probe.....	22
3	Contact Charge Dependence on Particle Diameter.....	30
4	Contact Charge in $\mu\text{C/g}$ for Particle Velocity 75 m/s.....	33
5	Charge Transfer for Particle Velocity 75 m/s.....	43

#### ACKNOWLEDGMENTS

We appreciate the interest, encouragement and suggestions contributed by John Nader, project officer for this work.

One of us, G. Reischl, on leave from I. Physikalisches Institut, University of Vienna, was supported in part by International Research Fellowship 1F05TW02271, National Institutes of Health.

## SECTION 1

### INTRODUCTION

The present project was undertaken in order to critically examine the basis for the indirect measurement of particulate matter mass concentration by means of contact electrification. The contact electrification monitor (1-6) offers some important advantages such as measurements in real time with a short response time. It is a mass monitor in that the electrical charge correlates accurately with the mass determined gravimetrically. (4,7,8,9) The instrument is relatively simple and the electrical signal is convenient for monitoring and data processing. The probe can be inserted directly into a stack to avoid the complications associated with extraction and external analysis.

In monitoring instruments based on contact electrification, a flow of the aerosol is directed at a probe. The transfer of charge from particle-probe collisions results in a current which is continuously monitored with a sensitive meter. Contact electrification, (10) which refers only to charge transferred between two bodies as a result of pure contact, will be used here to describe the charging process for the monitor, although sliding or rubbing may be present. Little is known about the latter charging mechanisms. We emphasize that no electrical potential is applied to the probe. The charge is transferred as a result of the contact potential between the two materials involved.

Although it has undergone over a decade of development, the contact electrification monitor is not widely used. This may be due to uncertainty arising from a lack of definitive data on the performance of the instrument and poor understanding of the charge transfer mechanism. However, because of the attractive advantages of this type of instrument, there is continuing interest in its development. For an account of the development of the theory and application of contact electrification to monitoring the reader is referred to the comprehensive review by John. (11)

In earlier work, John (9) tested the IKOR Air Quality Monitor<sup>\*</sup> in the laboratory with a variety of test dusts. The dynamic response was found to track well with that of an optical particle counter with the exception of an initial startup period of some 10 to 20 minutes during which the sensitivity increased towards the steady-state value. The total charge correlated well with gravimetric mass, as is required of a mass monitor. Humidity below saturation had no effect on the instrument. The electrical resistivity of the particle material was found to have a major effect on the sensitivity. Another important factor determining the sensitivity was the condition of the probe surface.

---

<sup>\*</sup> Manufactured by New IKOR, Inc., Gloucester, Mass. 01930.

The earlier work identified several areas needing further investigation. These included the influence of the probe surface condition on the sensitivity and the dependence of the contact charge on particle size. More generally, it was evident that there was a need for better understanding of the basic physical processes involved in contact charging so that the inherent limitations of the application to particulate monitoring could be assessed. The present project was designed to address these questions. First, preliminary measurements were made with the IKOR Monitor and monodisperse laboratory aerosol. Then apparatus and techniques were developed to allow investigation of the transfer of charge between particles and a probe surface under carefully controlled conditions. A theory was developed for the interpretation of the experimental results. Finally, the implications of the results for the application to monitoring were considered.

## SECTION 2

### CONCLUSIONS AND RECOMMENDATIONS

This investigation has provided extensive new experimental information on charge transferred by the impaction of particles on metal surfaces. A theoretical model has been found to account semi-quantitatively for the data. Thus a basic understanding of the charge transfer process has been achieved which can be applied to the development and assessment of the contact electrification monitor.

Experimental determination was made of the dependence of contact charging on particle size, impact velocity and electrical resistivity of the particle material. Contact charging was explored for insulating and conducting particles impacting on several different metals. The transfer of precharge was also investigated. The influence of the probe surface condition was explored.

The probe surface preparation procedure and the impaction probe design can be applied directly to practical monitoring. Implications of the various experimental and theoretical findings for monitoring have been discussed in detail. The monitor can produce a continuous relative measure of the mass flow. However, it must be calibrated for each source and recalibrated if the sampled material changes. The main uncertainty in the application of the monitor concerns the types of materials which can be sampled.

Future progress, both experimental and theoretical, on the basic charge transfer process will be difficult owing to the dependence on the unknown (and normally uncontrollable) properties of the particle and probe surfaces. The inherent limitations of the monitor restrict its usefulness to certain sources. Only field studies on specific sources can determine where the instrument can be applied.

## SECTION 3

### TESTS OF THE IKOR MONITOR

#### EXPERIMENTAL METHOD

The purpose of these tests was to investigate factors affecting the response of the IKOR Monitor to monodisperse laboratory aerosol. The IKOR Model 206 Portable Particulate Monitor with the standard bullet-shaped Inconel sensor was tested with monodisperse particles produced by a Berglund-Liu vibrating orifice aerosol generator. The experimental arrangement is shown in Figure 1. Particles from the aerosol generator were passed through the radiation from a Kr-85 source for charge neutralization. The aerosol then traversed an electrical mobility analyzer having parallel brass plates 12.7 cm x 31.8 cm, spaced 2.5 cm apart. Because the flowrate of the IKOR Monitor ranges up to 14 liters per second, clean dilution air was provided with a HEPA filter. The particle concentration and size distribution in the manifold were monitored with a Climet 201 Optical Particle Analyzer.

For some of the tests, the IKOR Monitor probe was inserted directly into the manifold. For other tests, the IKOR sensor and blower were separated as shown in Figure 1, to allow the placement of a Faraday cup between them. The Faraday cup consists of a 130 mm diameter high efficiency glass-fiber filter mounted in a metal housing. The housing is insulated by Teflon bushings and surrounded by a grounded metal shield. Charges stopping on the filter may flow directly to the metal housing or cause an equal charge to flow according to Gauss' Law. The current was monitored with a Keithley Model 616 Digital Electrometer. The arrangement of the IKOR components shown in Figure 1 is similar to the normal instrument configuration when the in-line filter is used for gravimetric determinations except that the filter is electrically insulated to permit the total current to be monitored.

#### RESULTS

##### Static Charging in the Teflon Hose

The IKOR Monitor is equipped with a flexible hose which connects the sampling probe to the sensing unit. The tube is lined with Teflon. A time-varying charging effect was traced to the flexible hose. With a steady aerosol flow, the charging effect caused a slow drift of the currents observed with the IKOR electrometer or the Faraday cup. Since this effect interferes with measurements, the flexible hose was replaced with a metal tube. The experience with the Teflon tube indicates the desirability of using grounded metal tubing to sample aerosol for charge measurements.

##### Response to Gaseous Ions

Using particle-free air from the aerosol generator and a total flowrate of  $14.1 \cdot s^{-1}$ , a current of  $2 \cdot 10^{-12} A$  was observed with IKOR Monitor and  $2.7 \cdot 10^{-11} A$  on the Faraday cup. When the Kr-85 source was removed, the IKOR

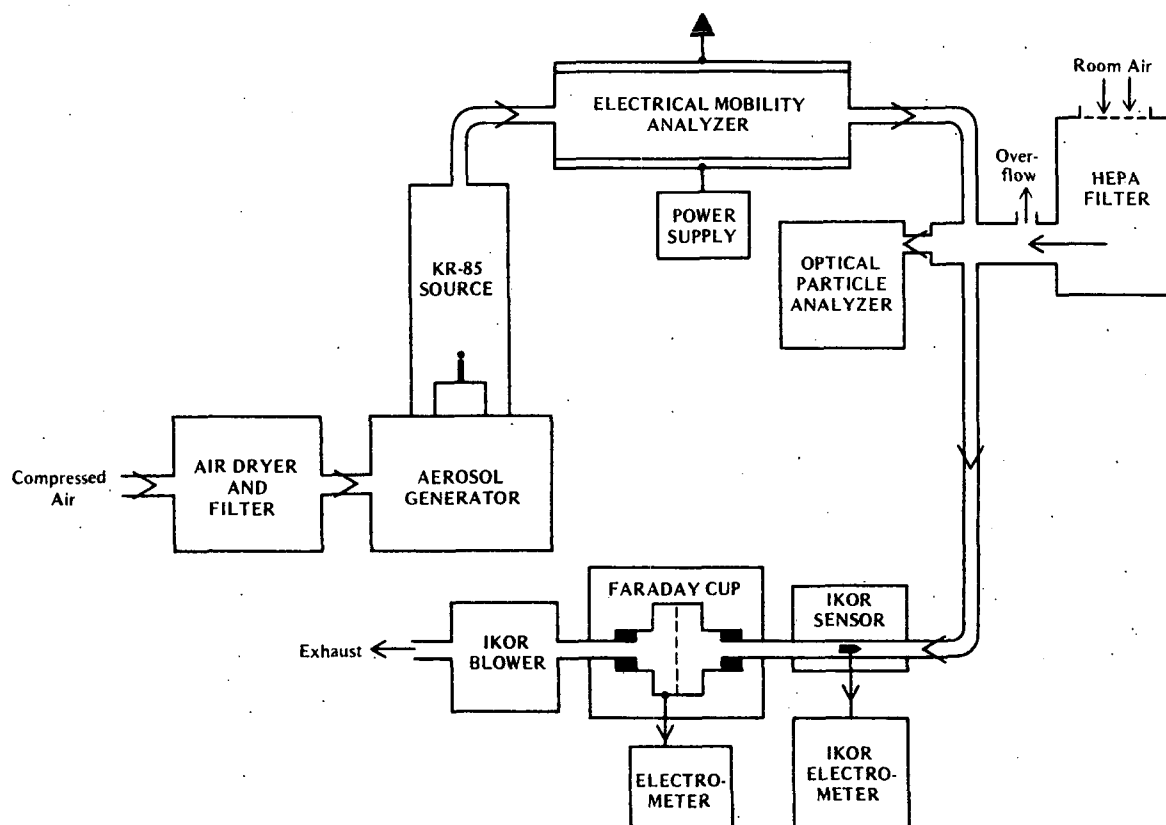


Figure 1. Experimental arrangement used for testing the IKOR monitor.

Monitor current was undetectable and the Faraday cup read  $1 \cdot 10^{-12}$  A. Thus, the IKOR Monitor responds to the gaseous ions created by the Kr-85 radiation. A net charge on the air can be produced by unequal losses of ions of opposite sign to the walls caused by differing diffusion constants.

The possibility that gaseous ions could be removed from the air stream by a transverse electric field was investigated. Particle-free air from the aerosol generator at a flowrate of  $100 \text{ l} \cdot \text{m}^{-1}$  was passed through the Kr-85 source radiation. A d.c. voltage was applied in steps to the plates of the electrical mobility analyzer and the current monitored on the Faraday cup which was placed directly after the mobility analyzer.

Surprisingly, the current was observed to increase from  $0.6 \cdot 10^{-11}$  A at 0 V to a maximum of  $2.6 \cdot 10^{-11}$  A at 20 V. Thereafter, the current decreased to zero at 63 V. At higher voltage, a negative current appeared. These observations indicate that the ions consist of a complex mixture of molecular species having a range of electrical mobilities. Removing ions of one sign causes an increase in the apparent current of the opposite sign.

Although the observed complications indicate need for caution in the setting of electric field intensity, a suitable field can greatly reduce the ion current. Since the monitor has been shown to respond to ions, this precaution is necessary.

#### Response to Precharge

Some tests were conducted with the Kr-85 source removed. Methylene blue particles were observed to cause negative currents in the IKOR Monitor and the Faraday cup. As a result of observations taken with and without the Kr-85 neutralizer, it was believed that the IKOR Monitor was responding to particle precharge (charge on the particles prior to contact with the probe). However, because of a number of uncertainties, the tests were not conclusive.

As a result of the data obtained in later experiments (described below) it is now known that the precharge on the methylene blue particles from the spraying process in the aerosol generator is considerably greater than the contact charge. Therefore, the IKOR Monitor was probably responding to the precharge.

#### IKOR Sensor Efficiency

Some measurements were made to ascertain the approximate efficiency of the IKOR sensor. One factor determining the efficiency is the probability that particles will impact on the probe. This was investigated by coating the probe with Dow Corning silicone vacuum grease to make the particles stick after impaction. Methylene blue particles were used so that the mass could be quantitated by dissolving the dye in alcohol-water solution and quantitating on a spectrophotometer. The total particle mass in the aerosol was measured by the use of an in-line glass fiber filter and quantitating by the same procedure. For  $4.5 \text{ } \mu\text{m}$  diameter particles, 5% of the mass was found on the sensor. For  $1.5 \text{ } \mu\text{m}$  particles, 9% was on the sensor.



Other data were provided by a comparison of the currents from the IKOR Monitor and the Faraday cup operated in series. A typical result is the following: for 3.9  $\mu\text{m}$  methylene blue particles generated with the Kr-85 source removed and at a flowrate of  $14 \text{ l}\cdot\text{s}^{-1}$ , the IKOR current was  $1.2\cdot 10^{-13}\text{A}$ ; the Faraday cup current was  $8.0\cdot 10^{-13}\text{A}$ .

These tests can be summarized by stating that the IKOR sensor efficiency for 1-5  $\mu\text{m}$  particles is approximately 10%. This is not surprising since the streamlined shape of the sensor facilitates the flow of aerosol around the sensor.

## SECTION 4

### CHARGE TRANSFER EXPERIMENTS

#### EXPERIMENTAL PROCEDURES

The preceding experiments with the IKOR Monitor revealed the need for the development of apparatus to allow observation of various charge transfer effects under controlled conditions. It is desirable to control the charge on the aerosol test particles. This includes charging or neutralizing the particles without producing gaseous ions. Further, it is desirable to observe the charge transfer between particles and probe with each particle colliding with the probe surface once and only once. An additional requirement is a probe configuration allowing changes of probe material and surface preparation.

The experimental arrangement developed for these measurements is shown as a block diagram in Figure 2. Particles from a Berglund-Liu vibrating orifice aerosol generator (12) could be charged or neutralized with a particle charger developed for this work. The aerosol then entered a chamber via the mobility analyzer (the voltage was normally off for this work); the particle concentration and size distribution were continuously monitored with a Climet 201 Optical Particle Analyzer. The aerosol was sampled from the plenum with an impaction probe especially designed for this work. The current from particle-probe charge transfer was monitored with a Keithley Model 616 Digital Electrometer. The aerosol was also sampled with the Faraday cup to determine the total charge on the aerosol. The flows through the impaction probe and the Faraday cup were maintained constant by Sierra\* mass flow controllers. Each of the principal components of the apparatus are discussed in more detail below.

#### Particle Charger

A technique was developed for the induction charging of droplets from the vibrating orifice aerosol generator. The induction electrode is shown in Figure 3 and Figure 4. By applying a d.c. voltage to the electrode, highly uniform charges of either sign can be placed on the droplets. After droplet drying, the charges are left on the residual particles. A typical calibration curve is shown in Figure 5 where the charge on 1.5  $\mu\text{m}$  diameter methylene blue particles is shown to vary linearly with the induction voltage. The intercept on the y-axis of the graph in Figure 5 represents the charge placed on the particles in the absence of applied voltage, which we call spray charge. The figure also illustrates the neutralization of the spray charge by cancellation with an opposing induction charge. In this case, approximately -2 V results in zero charge (intercept on x-axis).

---

\* Sierra Instruments, Carmel Valley, CA

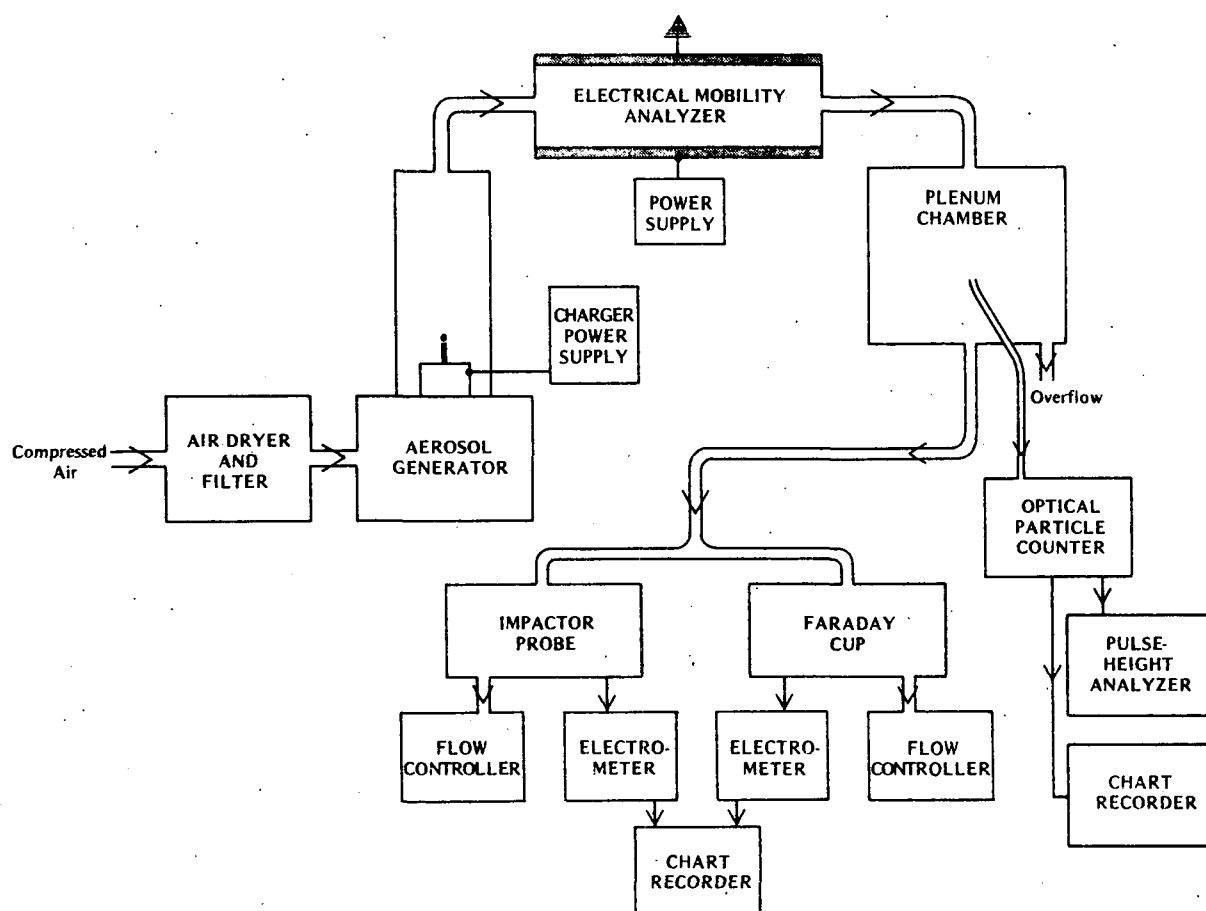


Figure 2. Experimental arrangement for charge transfer measurements

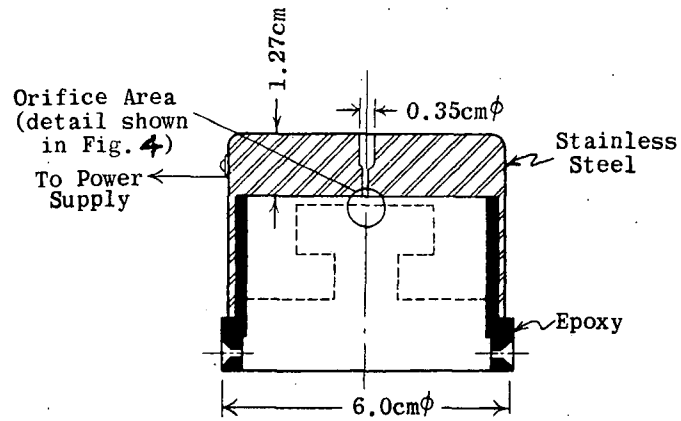


Figure 3. Apparatus for induction charging of particles from the vibrating orifice generator. The dotted lines outline the vibrating orifice assembly.

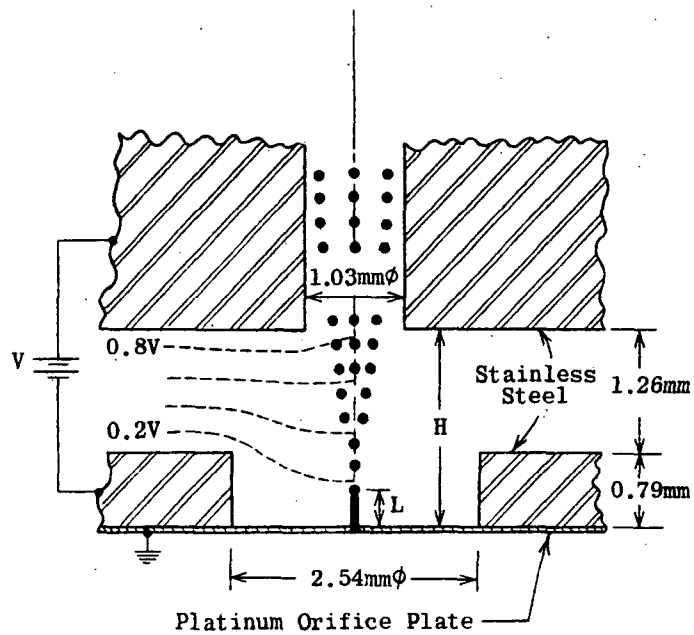


Figure 4. Detail of the area where the droplets are formed in the vibrating orifice generator.

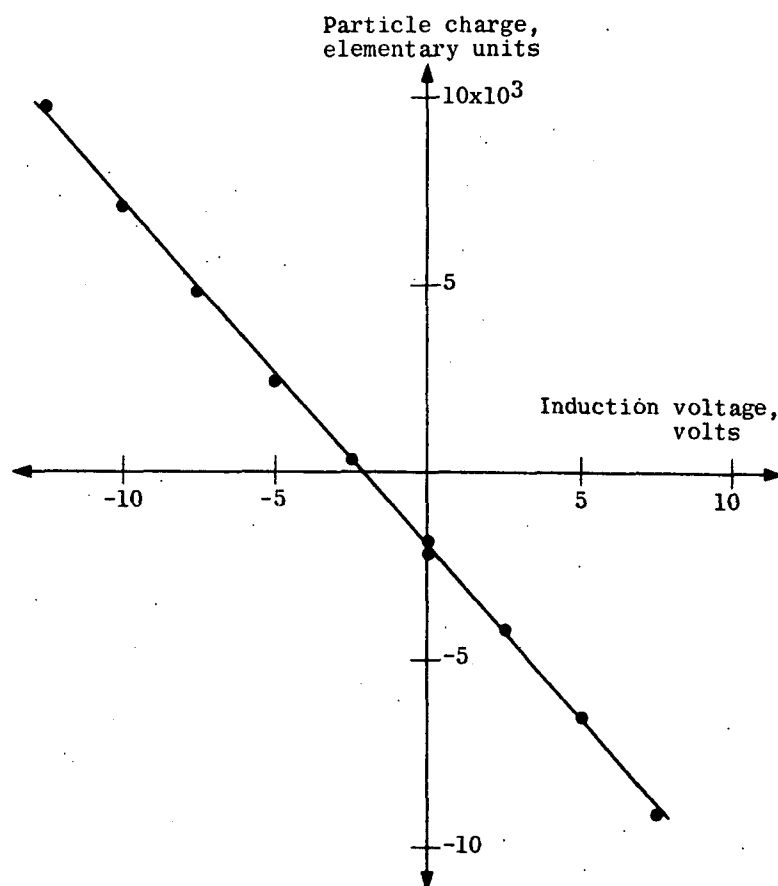


Figure 5. Typical calibration curve for the particle charger. These data were taken with 1.5  $\mu\text{m}$  methylene blue particles.

The induction technique places a uniform charge on the particles with almost instantaneous control of the magnitude of the charge. This includes neutralization of the charge. Moreover, no gaseous ions are produced. Additional details of the particle charger and some charging effects beyond the scope of the present work have been published (13).

### Particle Counting and Sizing

The particle sizes quoted here are the physical geometric diameters of the spherical particles. Particle sizing was based primarily on calculation from the known vibration frequency applied to the orifice, the liquid flow-rate and solute concentration. This was checked by sizing in a Zeiss microscope equipped with Epi (vertical) illumination. The optical particle analyzer served as a secondary standard and real time monitor of the mean size and size distribution. The particles were highly monodisperse, the geometric standard deviation being of the order of 1.02.

The optical particle counter sampled from the plenum. It was necessary to calibrate this particle count to the particle concentration sampled by the impaction probe and the Faraday cup. This was done by counting while simultaneously collecting particles on a high-efficiency filter in the Faraday cup. The methylene blue was then dissolved in alcohol-water solution and quantitated in a spectrophotometer. When a glass fiber filter was used it was found necessary to separate the fibers in a blender in order to extract all of the methylene blue. Ultrasonification was also useful. The slurry was then vacuum filtered through a glass frit to separate the solution from the glass fibers. When a Millipore membrane filter was used, both the filter and deposit were dissolved in acetone for quantitation. A similar calibration was carried out with the impaction probe. The particles deposited on the walls of the impactor were included in the analysis by washing it out with solvent.

### Faraday Cup

A Faraday cup was constructed to measure the charge on the particles. It consists of a filter surrounded by an aluminum cylinder connected to an electrometer (see Figure 6). The cup is insulated by Teflon and surrounded by a grounded aluminum shield. It should be noted that it is immaterial whether the charge collected on the filter is conducted to ground. The instant a charged particle enters the cup, an equal induced charge appears on the outside of the cup as required by Gauss' Law. This induced charge is removed and measured by the electrometer.

The Faraday cup shown in Figure 6 is our second model which incorporates several improvements over our first model (Figure 1). The principal features are listed below:

1. The parts are rigidly constructed to avoid the induction of currents by mechanical vibrations.
2. Teflon is used as the insulator. The surface exposed to the aerosol flow is kept small to avoid charging effects.

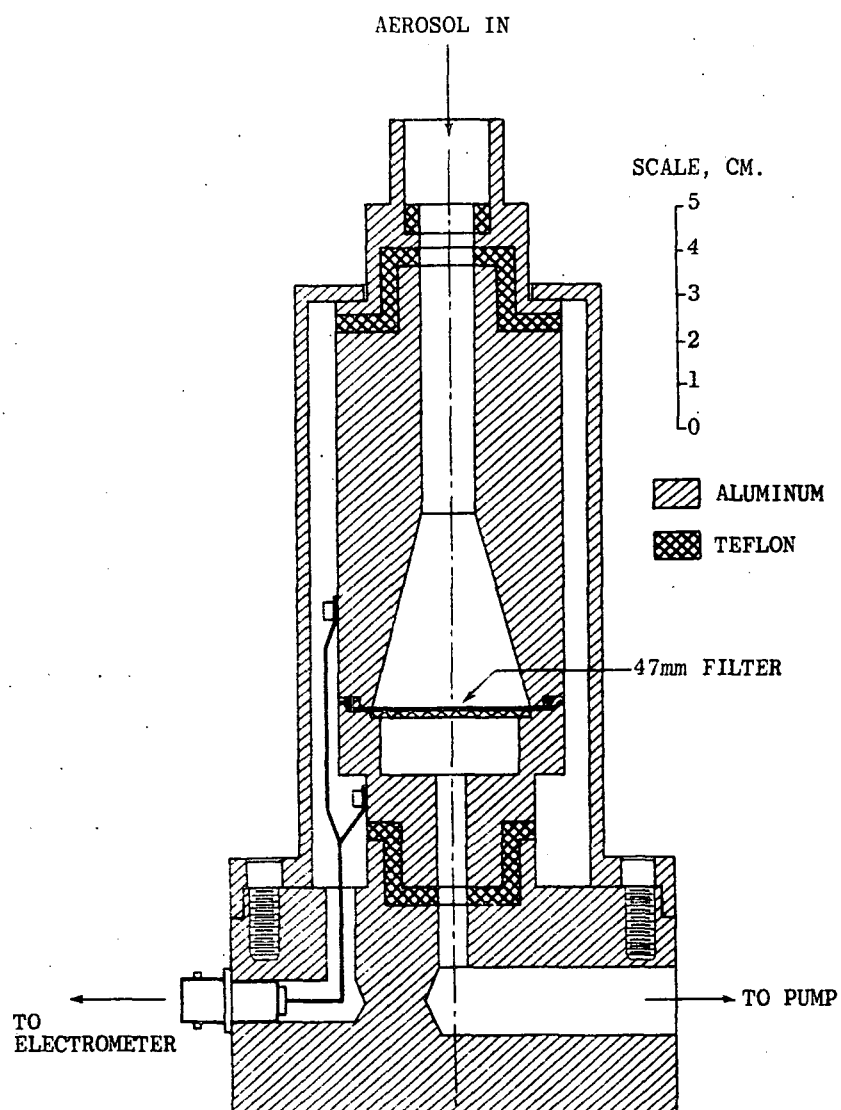


Figure 6. Faraday cup used to measure the electrical charge on particles.

3. The geometry is chosen to minimize leakage of electrical flux from the particles on the filter to the outside, and to minimize the pickup of flux from the outside. Backing the filter with a metal grid also helps in this regard. A coarse grid could be placed on top of the filter, but was not found necessary.
4. The taper on the cone leading to the filter was made with a  $15^\circ$  half angle, resulting in negligible particle loss to the walls. This simplifies the calibration procedure.
5. The top of the inner cylinder is removable to permit the filter to be changed. An O-ring seals to the metal and to the edge of the filter. Both top and bottom of the inner cylinder are directly connected to the electrometer.
6. The electrical resistance of the cup to ground was measured to be  $> 10^{14}$  ohms. Since the input resistance to the electrometer was only  $10^6$  ohms there was negligible leakage from cup to ground.

#### Impaction Probe

The impaction probe shown in Figure 7, is essentially a one stage inertial impactor with a rectangular slit. The air flow is maintained well above the particle cut off so that nearly all of the particles impact on the insulated probe surface. The top of the probe is beveled to eliminate multiple bouncing of particles.

The impaction probe shown in Figure 7 was our second, improved model. The first model was a modified Multi-day\* impactor. The slit width is 0.28 mm and the slit-to-probe distance 0.6 mm. Some important features of the design are:

1. The impaction efficiency is nearly 100% for particles with diameters greater than  $1 \mu\text{m}$  for the particle velocities used.
2. Multiple bouncing of particles is eliminated by the beveled probe surface and the sharpened slit edges.
3. The long taper on the inlet minimized particles losses.
4. The slit and probe assemblies are self-aligned to high precision but can be easily disassembled for cleaning.
5. The after filter permits a quantitative mass analysis and also microscopic examination of particles after impaction.
6. The interior of the apparatus has been shaped and polished to reduce the deposition of particles everywhere except on the after filter in order to facilitate the quantitative mass analysis of particles. This was only partially successful.

---

\* Sierra Instruments, Carmel Valley, CA



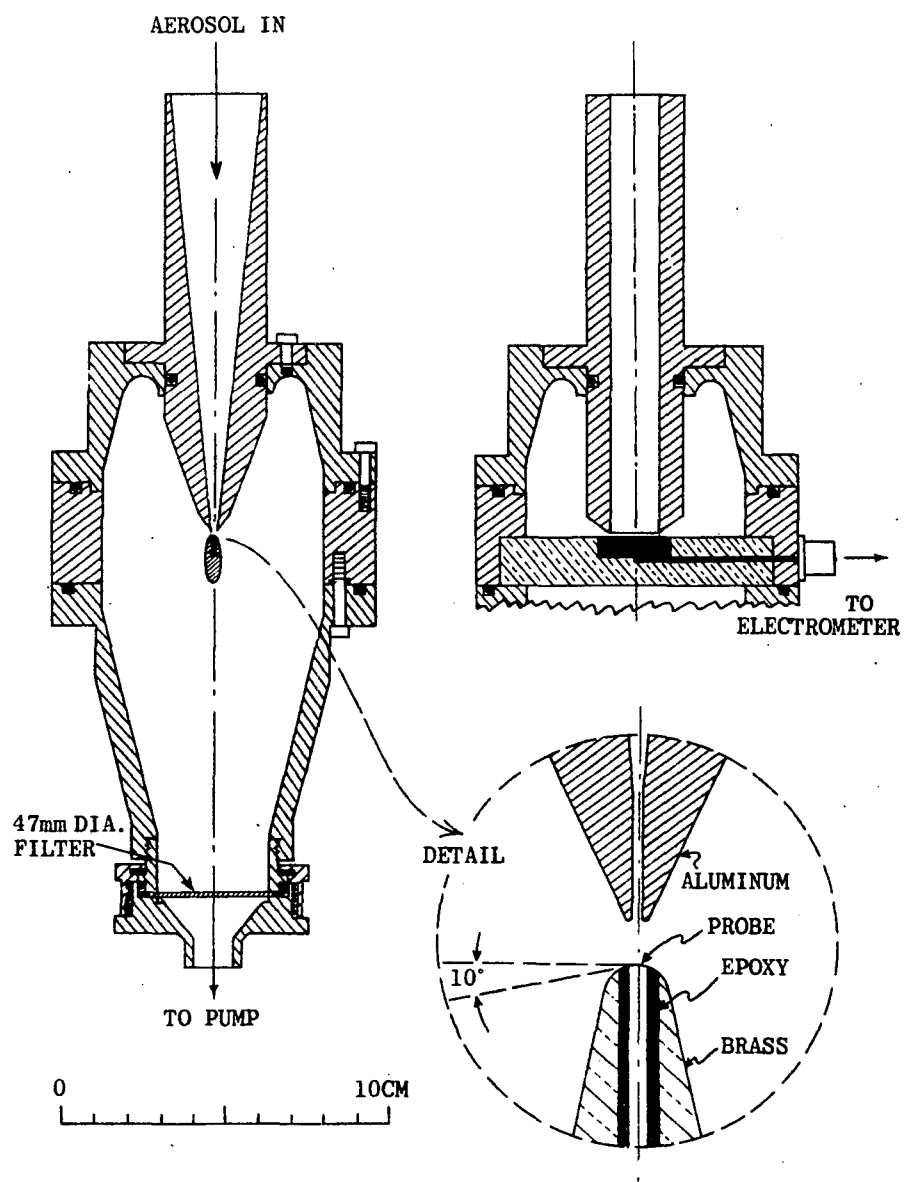


Figure 7. Impaction probe for charge transfer measurements.

7. The probe was designed to meet several requirements:

- a. The beveled upper surface should be highly polished and smoothly joined to the adjacent insulating and shielding materials.
- b. The probe should be electrically shielded except for the upper surface.
- c. The resistance to ground should be greater than  $10^8$  ohms.
- d. The electrical capacity should be minimized.
- e. The probe should be mechanically rigid to avoid the induction of currents.
- f. The area of exposed insulator should be minimized to avoid charging effects.
- g. The probe should be easily removed in order to facilitate cleaning and the substitution of other probe materials.

As shown in the detail on Figure 7, the probe has a rectangular exposed surface 0.051 cm wide by 2.22 cm long. It was inserted into a slot in the brass housing, shimmed with Teflon strips and the remaining space filled with a high-resistivity epoxy. A wire soldered to the bottom led to the electrometer connection. During the machining process, particles become imbedded in the surface of the epoxy, lowering the probe resistance to ground. However, it was found that the imbedded particles could be eliminated by a careful polishing procedure. Aluminum oxide powders were used with successively smaller grain size down to 0.05  $\mu\text{m}$  followed by rinsing with high purity water and baking at 110°C under vacuum.

#### Probe Surface Preparation--

For this work it is desirable to have a polished probe surface free of chemical contaminants and mechanical strains. These requirements correspond to those for the preparation of specimens for metallography. Therefore a similar procedure was adopted:

1. The surface is hand polished with Buehler\* Micropolish C (1.0 micron alpha alumina) and distilled water using a Buehler polishing cloth (Metcloth No. 407156). The surface is rinsed with distilled water.
2. Step 1 is repeated, but substituting Buehler Micropolish A (0.3 micron alpha alumina).
3. Repeat polishing but with Buehler Micropolish B (0.05 micron gamma alumina). After rinsing, the surface is checked under a microscope at 640X. If scratches are visible, steps 2 and 3 are repeated.

---

\* Buehler, Ltd., Evanston, Illinois

4. The surface is rinsed thoroughly with distilled water to remove all the alumina powder, and then scrubbed vigorously with a wet tissue paper (Kimwipe). It is then rinsed with water followed by isopropyl alcohol (reagent grade, filtered through 0.2  $\mu\text{m}$  Millipore membrane). The probe is then baked for 15 minutes at 70°C under vacuum to remove the alcohol.
5. After the probe is replaced in the apparatus, it is flushed with clean dry air for at least 20 minutes. This step appears to remove static charge effects from the insulator material surrounding the probe which has been affected by the cleaning procedure. The flushing also restores the probe to room temperature.
6. During subsequent use, if it was determined that the probe needed cleaning, it usually sufficed to repeat steps 4 and 5.

Probes were prepared of stainless steel, Inconel, titanium and platinum. The leakage resistance to ground, measured with a Keithley electrometer, ranged from  $10^{11}$  to  $> 10^{13}$  ohms. The background current with clean air was 5 to  $10 \cdot 10^{-15}$  A. When tested with methylene blue particles it was found that most of the particles bounce from the surface. Microscopic examination of the probe surface after exposure showed that only a few percent of the particles stick to the surface. For particles less than 4  $\mu\text{m}$  in diameter, the deposition on the walls of the impactor was less than 15% of the total, the remainder being deposited on the after filter.

#### Properties of the Particles Generated

Three types of particles were used in the present work, methylene blue, sodium chloride and potassium biphthalate. Methylene blue is an organic dye substance with both polar and nonpolar properties. Zinc-free methylene blue was dissolved in 50-50 isopropyl alcohol-water solution for atomization. The dried particles have a density of 1.343 and are smooth, spherical and bouncy. The dilution air in the aerosol generator was maintained at low humidity, producing methylene blue particles having a bright golden appearance under the microscope.

Sodium chloride was atomized from the aqueous solution. The morphology of the dried particles varied from fairly angular to nearly spherical depending on the size of the microcrystals in the aggregate particle. Examination of the deposit on the after filter of the impaction probe revealed the presence of crystalline fragments of particles indicating that a significant fraction of the sodium chloride particles break up during the impaction.

Potassium biphthalate was atomized from aqueous solution, producing smooth, white, spherical particles. When sampled with an inertial impactor these particles prove to be quite bouncy, i.e., they show very little tendency to stick to the impaction surface.

#### MEASUREMENTS

##### Effect of Probe Surface Preparation on Charge Transfer

The probe surface preparation procedure described above is the final version developed as a result of preliminary tests. It is instructive to review the data obtained with various surface treatments. Figure 8 shows

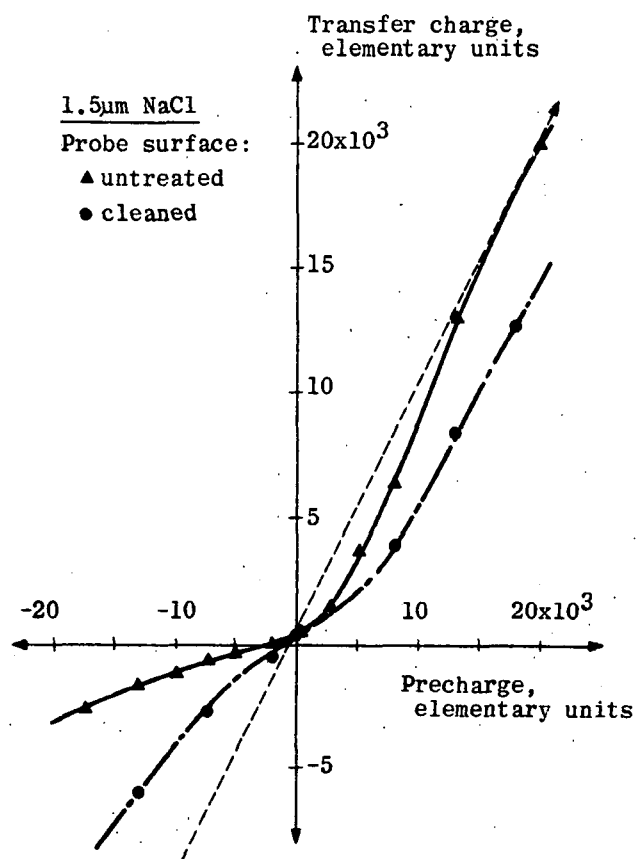


Figure 8. Charge transferred to the stainless steel probe as a function of the particle precharge. The dashed line corresponds to complete charge transfer. These preliminary data were taken to investigate surface cleaning effects.

charge transfer curves for 1.5  $\mu\text{m}$  diameter sodium chloride particles and the stainless steel probe. The charge per particle transferred to the probe is plotted as a function of the precharge on the particles. These charge transfer curves are nonlinear. Interestingly, the curve for the untreated probe surface shows that positive charge is more readily transferred than negative, i.e., there is a rectifying action. To investigate the possible role of surface contaminants, the probe was cleaned with isopropyl alcohol and Kimwipes. The charge transfer curve for the "cleaned" probe is symmetric with respect to charge sign, although charge transfer in the "forward" direction (positive charge) was lowered by the cleaning. The contact charge is simply given by the y-intercept of the charge transfer curve which corresponds to zero precharge. We note that the contact charge for NaCl on stainless steel is positive; further, the contact charge was relatively unaffected by the surface treatment in this case.

These observations establish the importance of the surface condition of the probe for charge transfer. Even the mild cleaning had a large effect on the charge transfer. The cleaning removed some surface contaminants (the rectifying action suggests an oxide layer) but also apparently left a film inhibiting some charge transfer. Thus, the investigation of charge transfer cannot be separated from the question of probe surface condition. The transfer of precharge, however, provides a sensitive tool for the assessment of the surface condition. Additional data were taken to investigate various probe treatments. Some results are shown in Figure 9 and Figure 10 for methylene blue particles. The curves are nonlinear and vary considerably. We note that the contact charge for methylene blue is affected by the surface treatment. Data related to surface treatments are summarized in Table 1 and Table 2.

Finally, a cleaning procedure was devised which gave reproducible results. This procedure, which involves polishing the probe as described above, produces linear charge transfer curves. (See Figure 11 and Figure 12) After a polishing, the probe yields good data for a period of time. The duration of this period was not determined by the present work, but exceeds several hours. As previously noted, the transfer of precharge is more sensitive to surface condition than the contact charge. Thus, some contact charge data taken with only an alcohol, water, and tissue cleaning were consistent with data taken with a freshly polished surface. (See Figures 13 and 14).

#### Currents from Gaseous Ions

The contact charge is defined as the charge transferred to the probe by a particle which is initially uncharged. In the initial phases of this work, the particles were neutralized (Boltzmann equilibrium charge distribution) by passing the aerosol through the radiation field of a Kr-85 source. However, a current was observed from the impaction probe and Faraday cup even in the absence of particles. This current was traced to residual ions from the Kr source. The current varied as a function of voltage applied to the mobility analyzer (Figure 2), in sign as well as magnitude, indicating the presence of a complex bipolar mixture of ions having various mobilities. At any given voltage on the mobility analyzer, the net charge was observed downstream. It was found that an electric field of 60 V/cm was sufficient to remove essentially all of the ions. Such a field is too small to remove an appreciable number of aerosol particles. These observations definitely established that the impaction probe responds to gaseous ions.

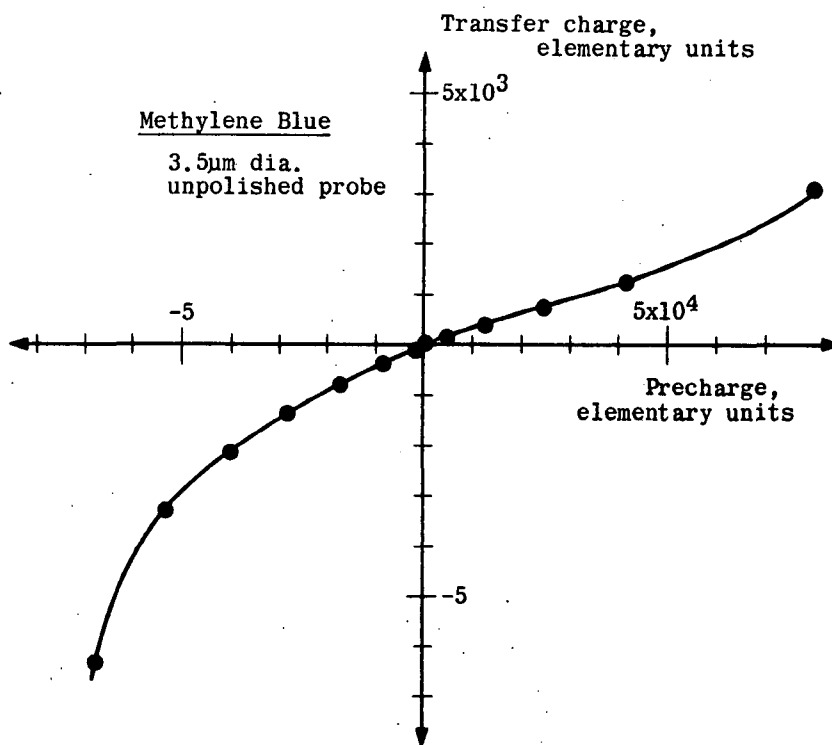


Figure 9. Charge transfer curve for methylene blue particles impacting on an unpolished stainless steel probe showing nonlinear charge transfer and anomalous contact charge.

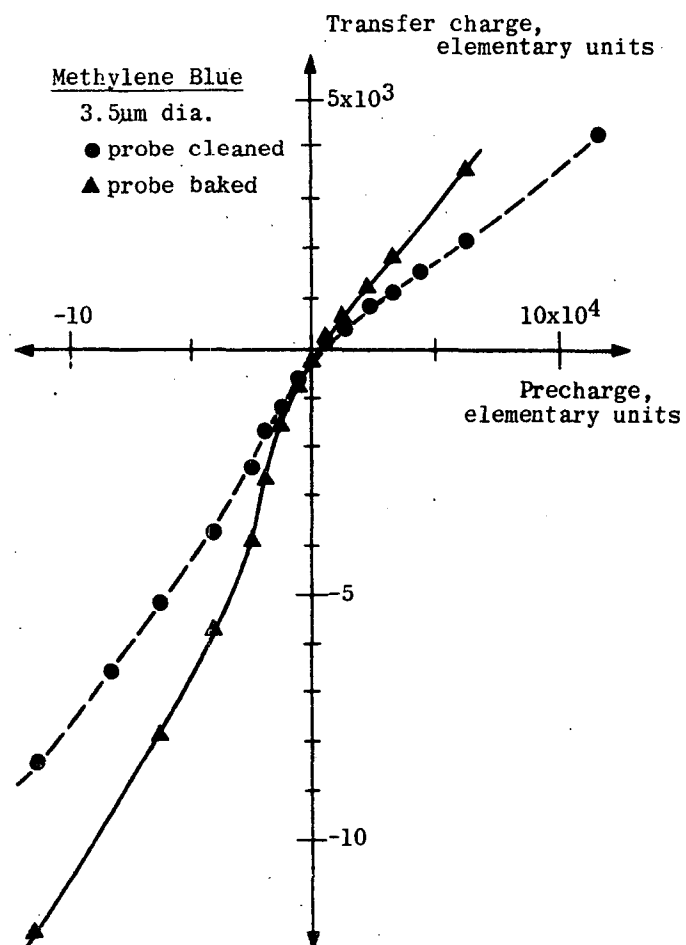


Figure 10. Nonlinear charge transfer curves obtained with two different surface treatments on a stainless steel probe.

TABLE 1. CONTACT CHARGE FOR SODIUM CHLORIDE PARTICLES IMPACTING AT 71 m/s  
ON A STAINLESS STEEL PROBE

Particle Diameter $\mu\text{m}$	Probe Surface Treatment	Contact Charge el. chg./particle
1.5	Untreated	380
2.5	Untreated	1025
3.5	Untreated	2850
5.0	Untreated	5800
1.5	Cleaned*	300
3.5	Cleaned*	3250

\*Cleaned with isopropyl alcohol and Kimwipes

TABLE 2. CHARGE TRANSFER DATA FOR METHYLENE BLUE PARTICLES IMPACTING AT  
71 m/s ON A STAINLESS STEEL PROBE

Particle Diameter, $\mu\text{m}$	Probe Surface Treatment	Contact Charge el. chg./particle	Transfer Charge Precharge	
2.5	Polished*	- 174	0.0375	} av. 0.031 $\pm 0.013$
3.0	Polished*	- 280	0.0300	
3.0	Polished*	- 260	0.0460	
3.5	Polished*	- 500	0.0108	
3.5	Polished*	- 470	0.0300	
2.5	Unpolished	$\sim 0$	Nonlinear	
3.5	Unpolished	$ Q_c  < 100$	Nonlinear	
3.5	Baked 36 h.	- 200	Nonlinear	
3.5	Chem. cleaned <sup>†</sup>	- 150	Nonlinear	
3.5	Chem. cleaned <sup>#</sup>	$ Q_c  < 240$	Nonlinear	

\*Polishing procedure described in text.

<sup>†</sup>Cleaned with surface active agent, RBS 25, Pierce Co. Rockford, Ill.

<sup>#</sup>Cleaned with RBS 25, isopropyl alcohol, Kimwipes.



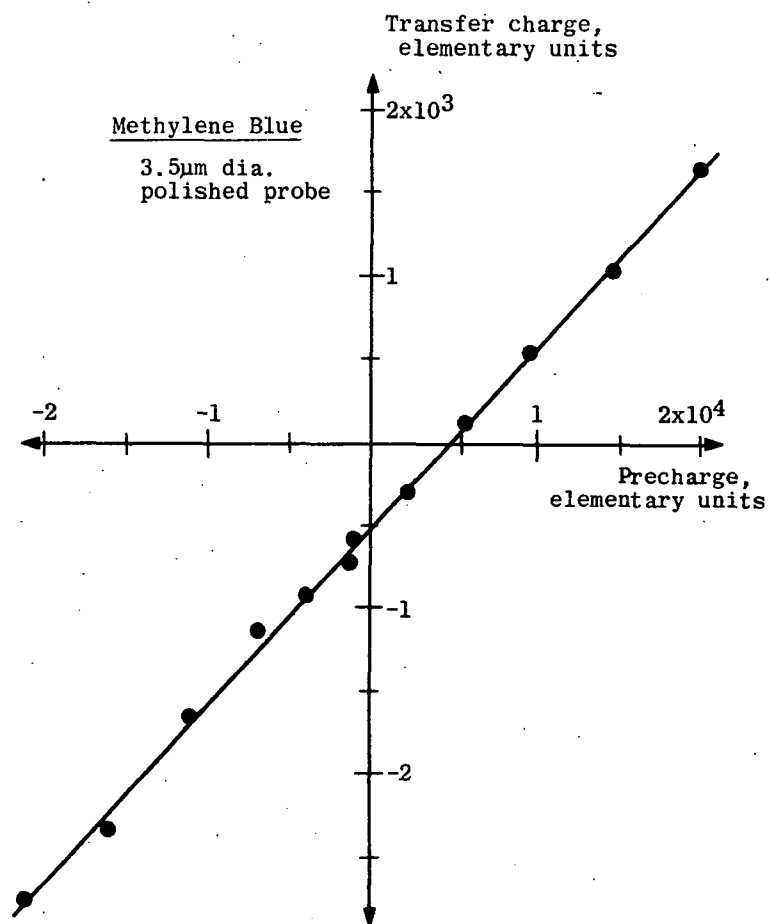


Figure 11. Linear charge transfer curve obtained with the stainless steel probe polished by the procedure described in the text.

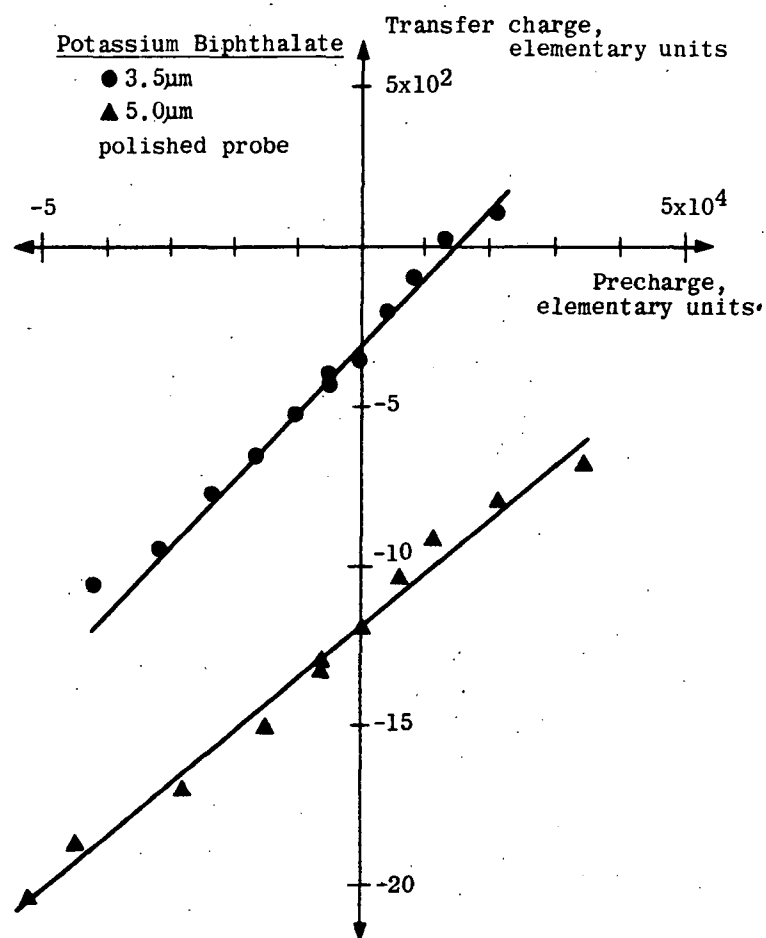


Figure 12. Charge transfer data obtained with potassium biphthalate particles and a polished stainless steel probe.

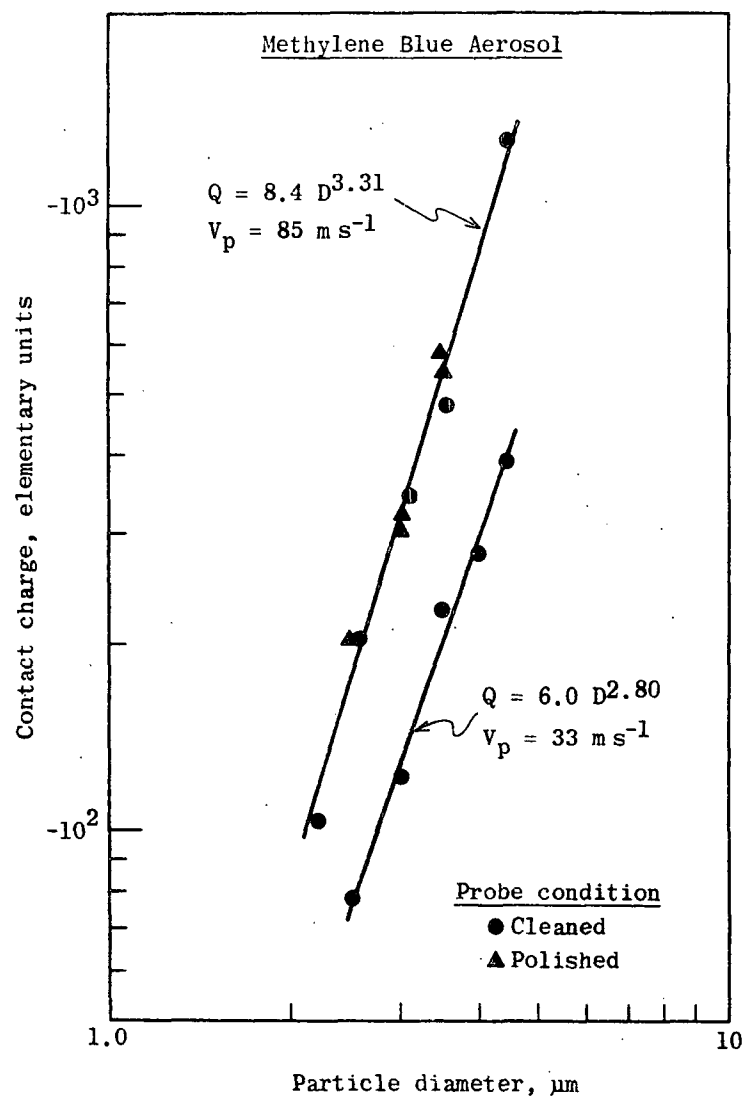


Figure 13. Contact charge vs. particle diameter for methylene blue particles impacting on a stainless steel probe at two different particle velocities. The lines are fitted to the data by least squares. This plot indicates that the contact charge is less sensitive to probe surface condition than is precharge (Fig. 10).

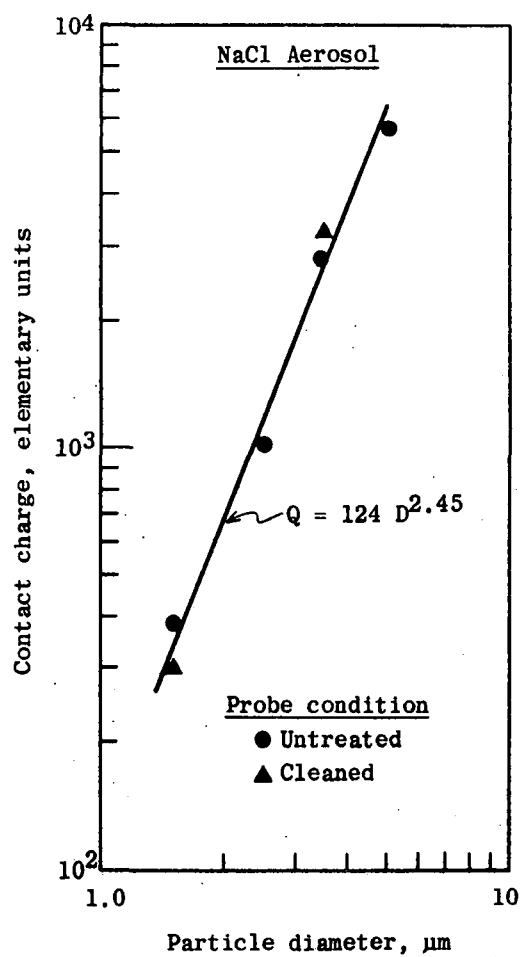


Figure 14. Contact charge vs. particle diameter for sodium chloride particles impacting on a stainless steel probe.

### Contact Charge Dependence on Particle Size

Data on the effect of particle size on the contact charge are valuable for understanding of the physical mechanism of the charging process and have important implications for the application to monitoring. The particle size dependence was investigated by measuring the contact charge for monodisperse particles of methylene blue, sodium chloride and potassium biphthalate impacting on the stainless steel probe and for methylene blue impacting on the titanium probe.

The initial measurements were made with methylene blue particles neutralized by the Kr-85 source. The current from the impaction probe was integrated with the electrometer to obtain the total charge which was then divided by the number of particles. The latter was determined by dissolving the deposits in the impactor, quantitating on the spectrophotometer and dividing by the average volume of a particle. Results are shown in Figure 13 for two different particle velocities and for two different probe surface treatments. Most of the other measurements were made by neutralizing the particles with the induction charger or by taking the intercept of the charge transfer curve. Particle number was based on the optical particle count with the calibration determined by spectrophotometry of the deposit. Results are shown in Figures 14-16. The lines were fitted to the data by the method of least squares.

Each set of data points is well fitted by a straight line on the log-log plots indicating that the contact charge depends on the particle diameter raised to an exponent approximately equal to three. The data are summarized in Table 3. Judging from the methylene blue data, the exponent does not vary significantly with particle velocity or probe material. Relative to methylene blue the exponent is slightly lower for sodium chloride and slightly higher for potassium biphthalate. However, the accuracy of the data is not sufficient to conclude that the differences are significant. The measurements are difficult because of the strong dependence of the contact charge on particle diameter.

The weighted average value of the exponent for all the measurements except sodium chloride is  $3.04 \pm 0.08$ . Therefore the contact charge is essentially proportional to the cube of the particle diameter or equivalently, to the particle volume or mass. This result will be further discussed in terms of a theoretical model below. We note that the cube law implies that the contact charge from sampling a number of particles of the same material will be proportional to the total mass of the particles, independent of the particle size distribution. Thus we have established that on a microscopic (particle by particle) basis the contact electrification monitor is a mass monitor.

### Contact Charge Dependence on Particle Velocity

The particle impact velocity was varied by changing the air flow rate in the impaction probe. The resulting data for methylene blue particles impacting on the stainless steel probe is shown in Figure 17. The data are well fitted by straight lines through the origin indicating that the contact charge is proportional to the velocity. Combined with the preceding result that the contact charge is proportional to the mass, this implies that the contact charge is proportional to the momentum of the particle.

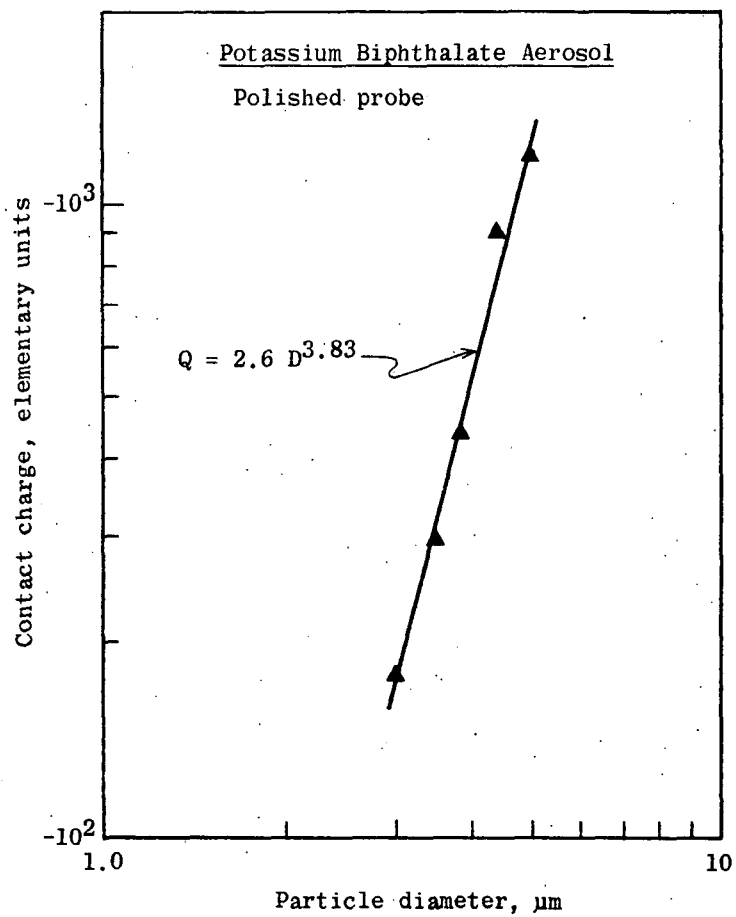


Figure 15. Contact charge vs. particle diameter for potassium biphthalate particles impacting on a stainless steel probe.

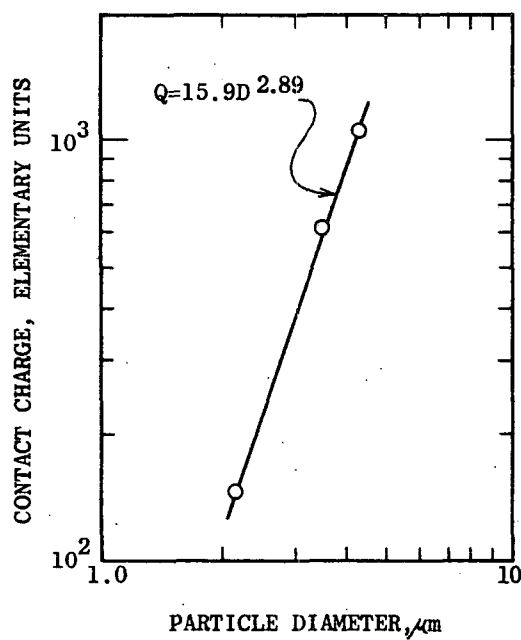


Figure 16. Contact charge vs. particle diameter for methylene blue particles impacting on a titanium probe.

TABLE 3. CONTACT CHARGE DEPENDENCE ON PARTICLE DIAMETER

Particle	Probe	Particle Velocity	Exponent, Std. Dev.
Methylene blue	Stainless Steel	85 m/s	$3.31 \pm 0.16$
Methylene blue	Stainless Steel	75 m/s	$2.90 \pm 0.15$
Methylene blue	Stainless Steel	33 m/s	$2.80 \pm 0.16$
Sodium chloride	Stainless Steel	50 m/s	$2.45 \pm 0.14$
Potassium bi-phthalate	Stainless Steel	85 m/s	$3.83 \pm 0.27$
Methylene blue	Titanium	75 m/s	$2.89 \pm 0.16$
Weighted average $3.04 \pm 0.08$ (Excluding sodium chloride)			



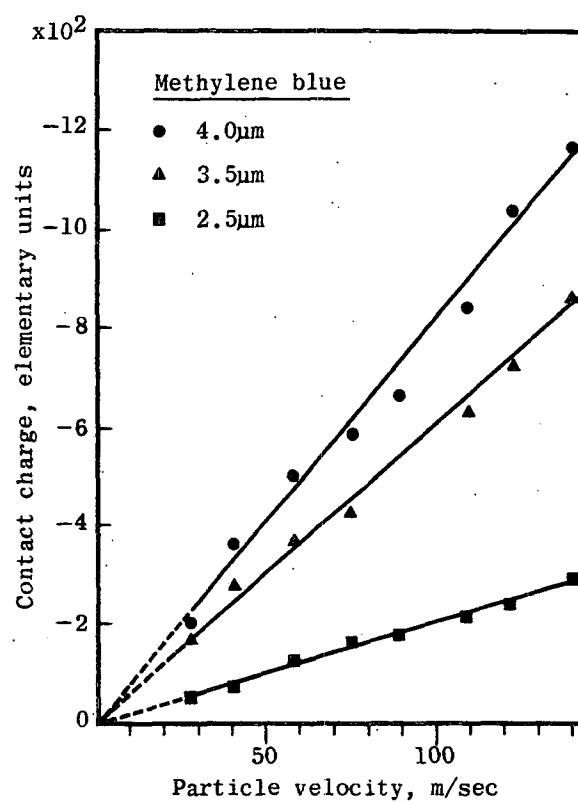


Figure 17. Contact charge vs. particle velocity for methylene blue particles impacting on stainless steel.

### Contact Charge for Several Particle and Probe Materials

The contact charge was measured for methylene blue, potassium biphthalate and sodium chloride particles impacting on stainless steel, Inconel, titanium and platinum probes. By using the cube law and the particle density the results were expressed in terms of charge per mass and listed in Table 4. The stainless steel probe data were taken at 85 m/s and corrected to 75 m/s, assuming the proportionality to velocity established above.

The data are also shown graphically in Figure 18. In both Table 4 and Figure 18 the data are arranged to display the trends. Considering probe material, the absolute magnitude of the contact charge generally increases in order from stainless steel to Inconel, titanium and platinum. The difference between Inconel and titanium was small, however. The absolute value of the contact charge increased generally in the order methylene blue, potassium biphthalate and sodium chloride. The contact charge was always negative for methylene blue and potassium biphthalate and positive in the case of sodium chloride except for the anomalous negative value obtained with the platinum probe. The considerable variation of the contact charge/mass with materials is evident.

### Transfer of Precharge

The transfer of precharge from particle to probe was discussed above in connection with the probe surface preparation and plots were shown in Figures 11 and 12. Additional examples of charge transfer for various particle and probe materials are shown in Figures 19, 20, 21 and 22. All of the data show linear charge transfer, however, Figures 20, 21 and 22 require lines with different slopes depending on the sign of the precharge. Additional cleaning of the probe did not result in equal slopes (single straight line plot as in Figure 19). Other examples of the type of Figures 20-22 were encountered as the particle-probe combinations were varied, in fact, it appears that this type of plot is more common than the single straight line. Figures 20-22 show a systematic effect which was observed in all the measurements which were not fitted by a single straight line. When the contact charge is positive (intercept on positive y-axis) the slope is greater for positive precharge (positive x-axis). Similarly when the contact charge is negative, the slope is greater for negative precharge. As will be discussed later, this effect is very similar to the action of a biased p-n junction.

The linear charge transfer curves were obtained after the probe was polished and cleaned according to the established procedure. However, during the initial exposure to a given aerosol, the charge transfer varied before approaching an asymptotic value over a period of 20 to 60 minutes. Some illustrative data is shown in Figures 23-26. It can be seen that prior exposure to a different aerosol can drastically affect the early time dependence of the transfer charge. The procedure adopted for taking charge transfer data with a given aerosol was to first expose the probe to the aerosol until the asymptotic region was reached.

For each combination of particle and probe materials the ratio of transfer charge to precharge was determined from the slope of the charge transfer line. The data are summarized in Table 5. Unlike the contact charge, the fraction of precharge transferred does not appear to depend on

TABLE 4. CONTACT CHARGE\* IN  $\mu\text{C/g}$  FOR PARTICLE VELOCITY 75 m/s

Probe	Particle Material		
	Methylene blue	Potassium biphthalate	Sodium chloride
Stainless Steel	$- 2.7 \pm 0.1$	$- 1.9 \pm 0.1$	$+ 8.0 \pm 0.6$
Inconel	$- 1.1 \pm 0.2$	$- 2.7 \pm 0.6$	$+ 25 \pm 4$
Titanium	$- 3.6 \pm 0.5$	$- 6.9 \pm 0.3$	$+ 24 \pm 2$
Platinum	$- 3.4 \pm 1.6$	$- 20 \pm 3$	$- 75 \pm 5$

\*Charge transferred to the probe.

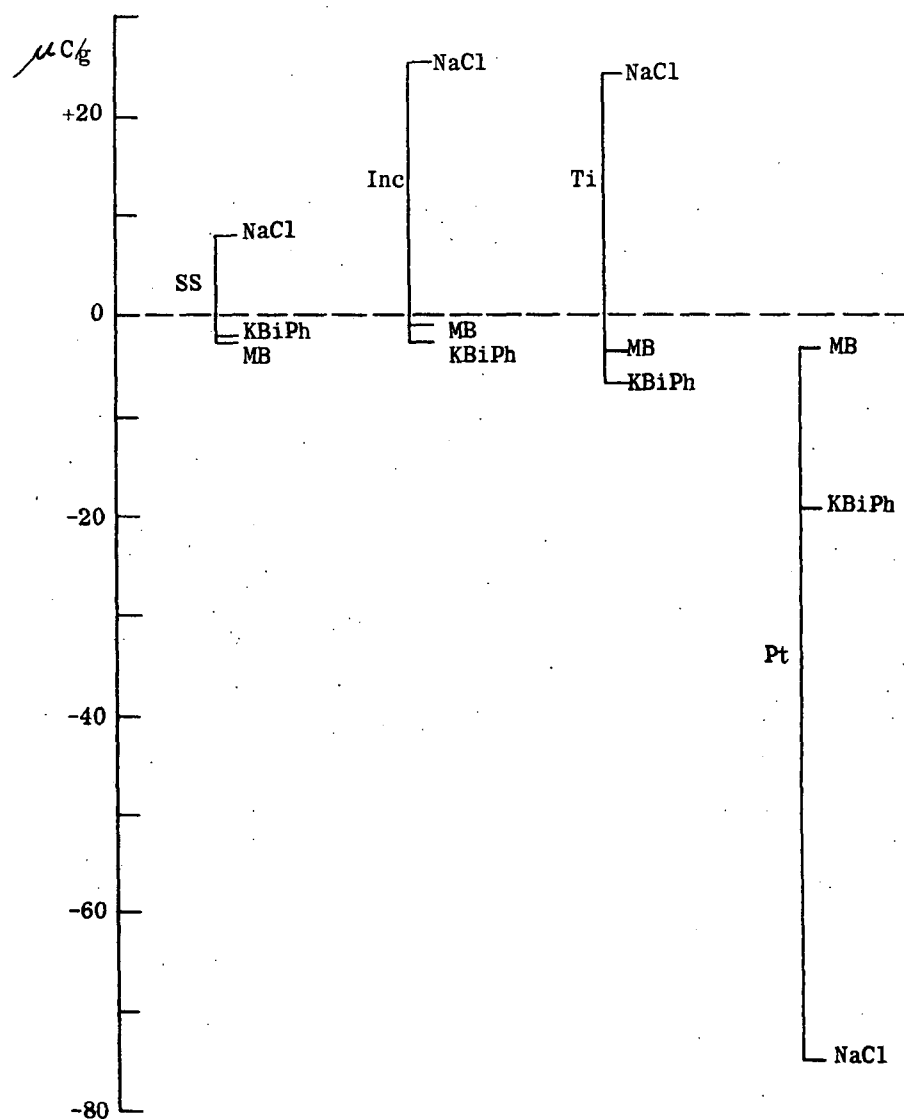


Figure 18. Contact charge/mass for various materials. Particle materials are: NaCl-sodium chloride, KBiPh-potassium biphthalate, MB-methylene blue. Probe materials are: SS-stainless steel, Inc-Inconel, Ti-titanium, Pt-platinum.

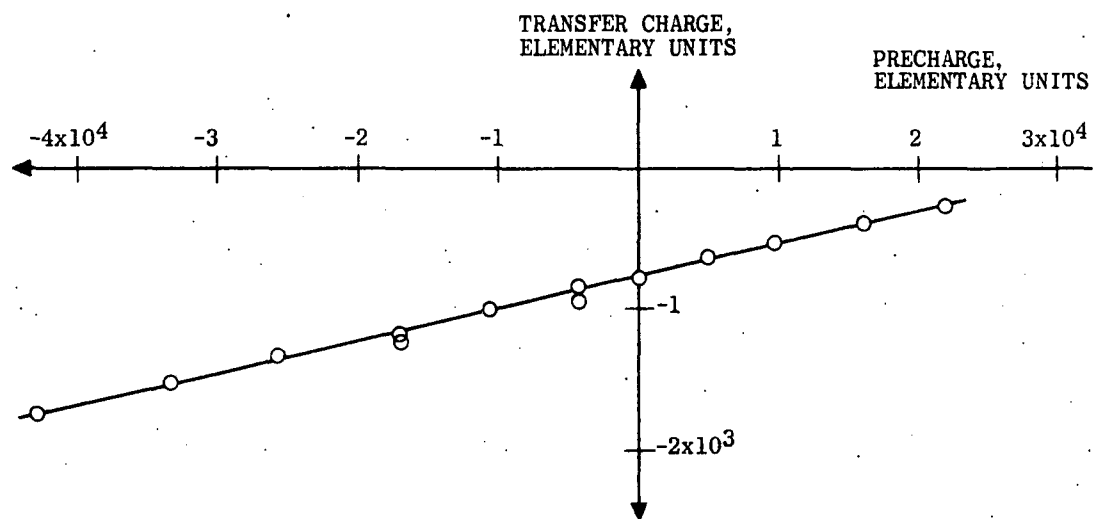


Figure 19. Charge transfer for 2.78  $\mu\text{m}$  potassium biphthalate particles impacting on a titanium probe.

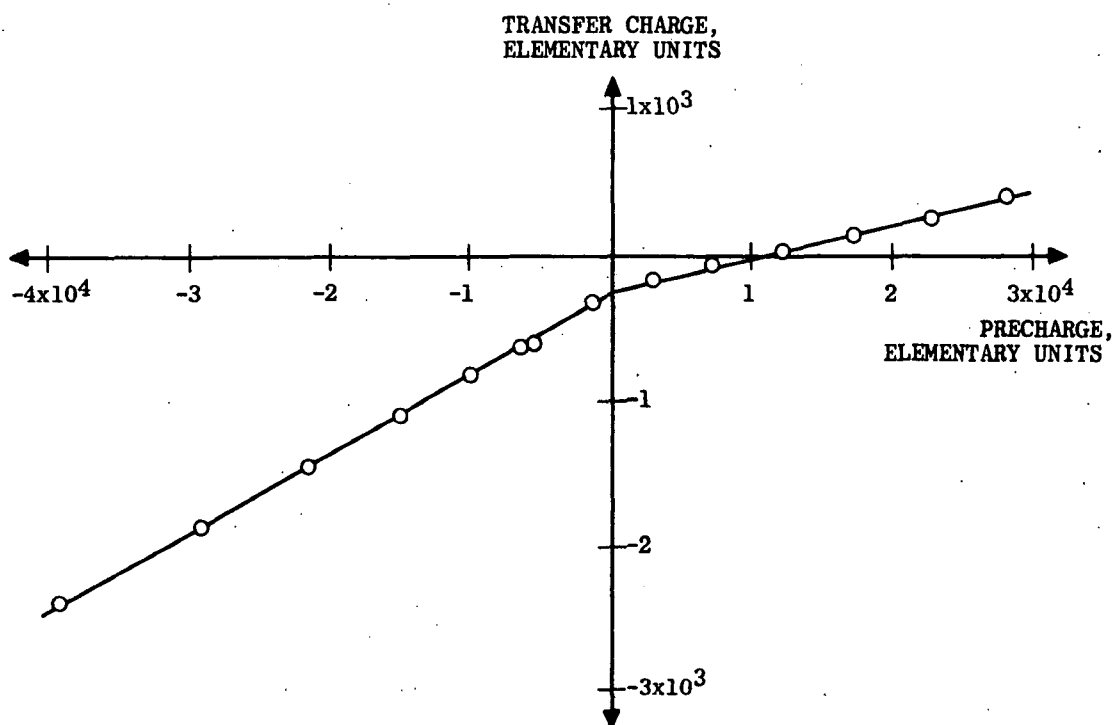


Figure 20. Charge transfer for 2.78  $\mu\text{m}$  potassium biphthalate particles impacting on an Inconel probe.

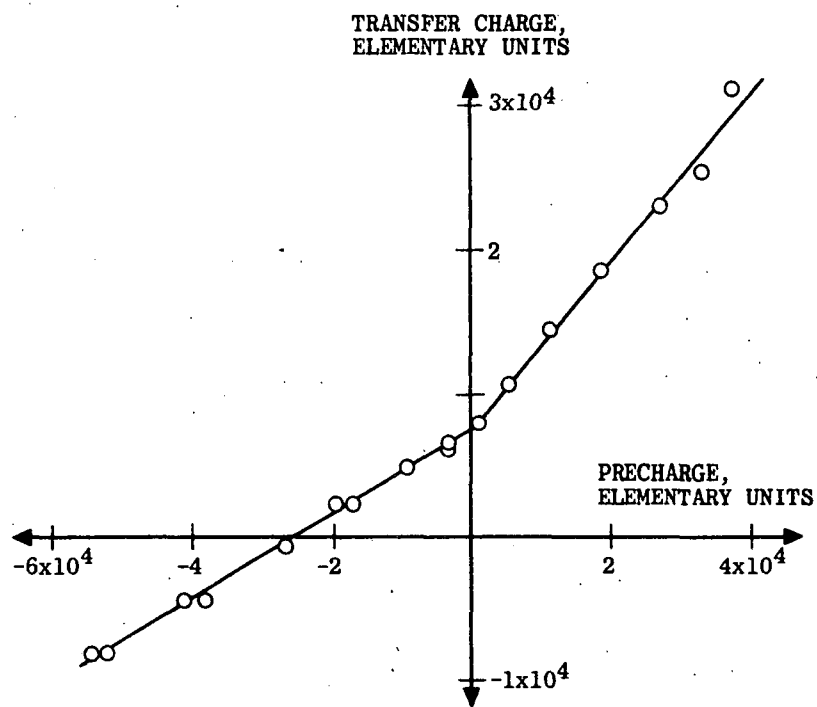


Figure 21. Charge transfer for 3.5  $\mu\text{m}$  sodium chloride particles impacting on a titanium probe.

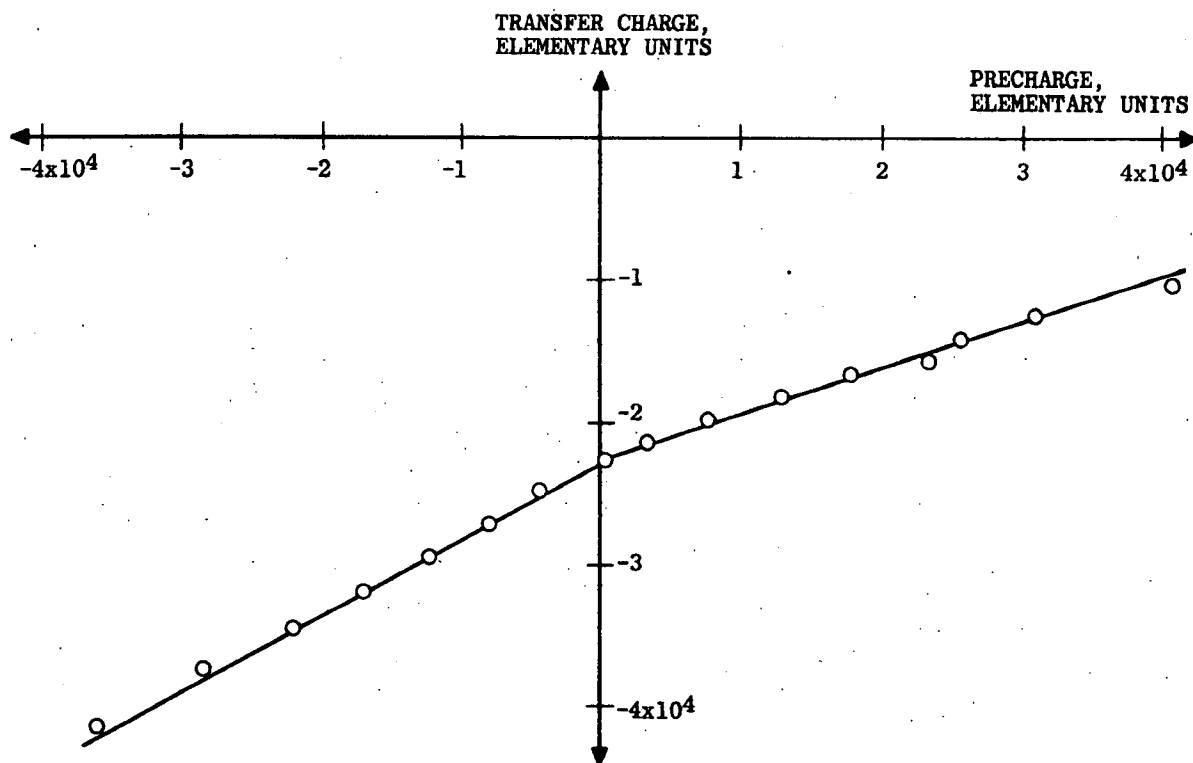


Figure 22. Charge transfer for 3.5  $\mu\text{m}$  NaCl particles impacting on a platinum probe.



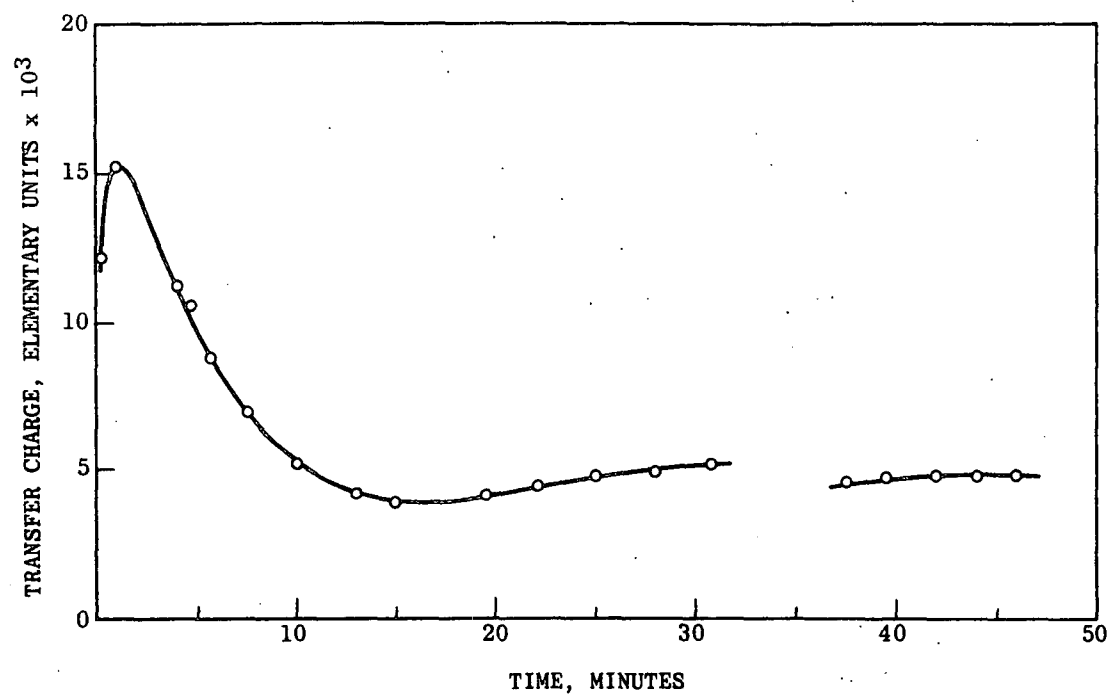


Figure 23. Time dependence of transfer charge from 3.5  $\mu\text{m}$  NaCl particles with a precharge of -5640 elementary charges to a freshly polished titanium probe. The aerosol generator was interrupted from 32-37 minutes.

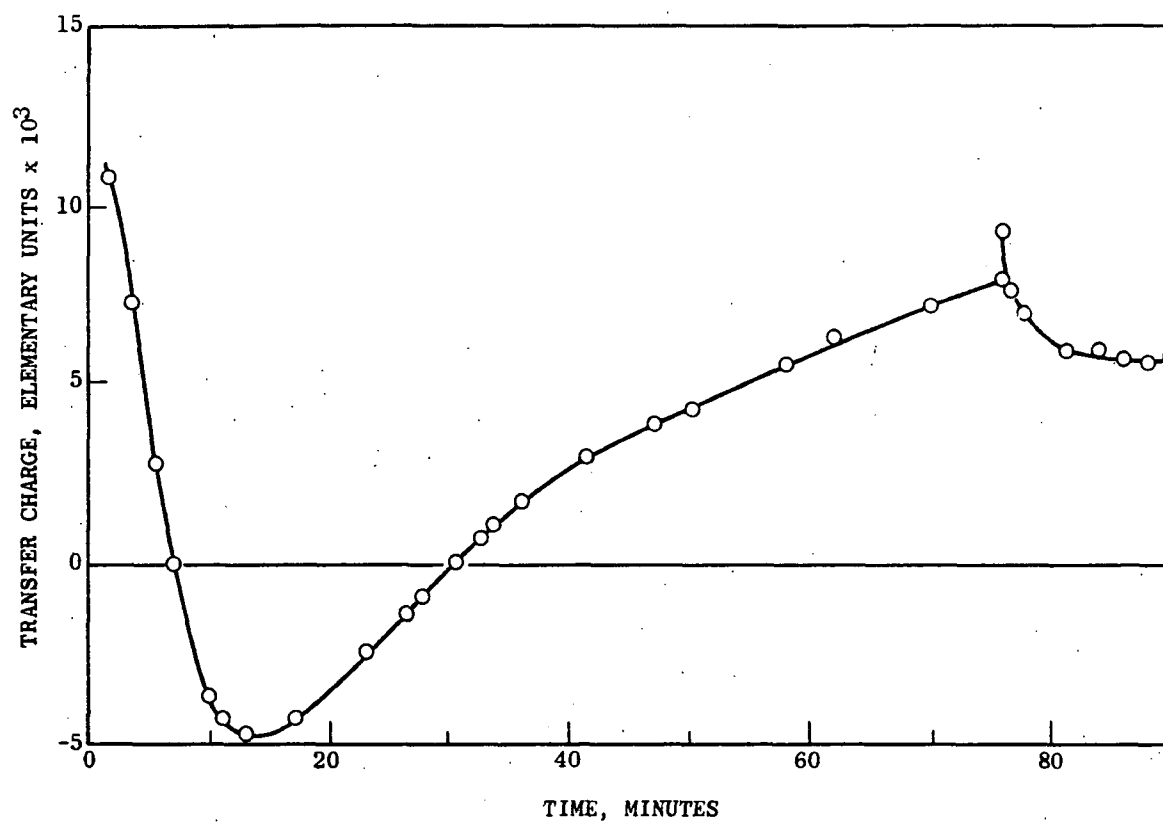


Figure 24. Same as Figure 23 except for the probe exposure history. Following the NaCl run shown in Figure 23, the probe was exposed to potassium biphthalate particles for about one hour and then to NaCl particles for 0.5 hour. It was then cleaned with alcohol and water before starting the above NaCl run.

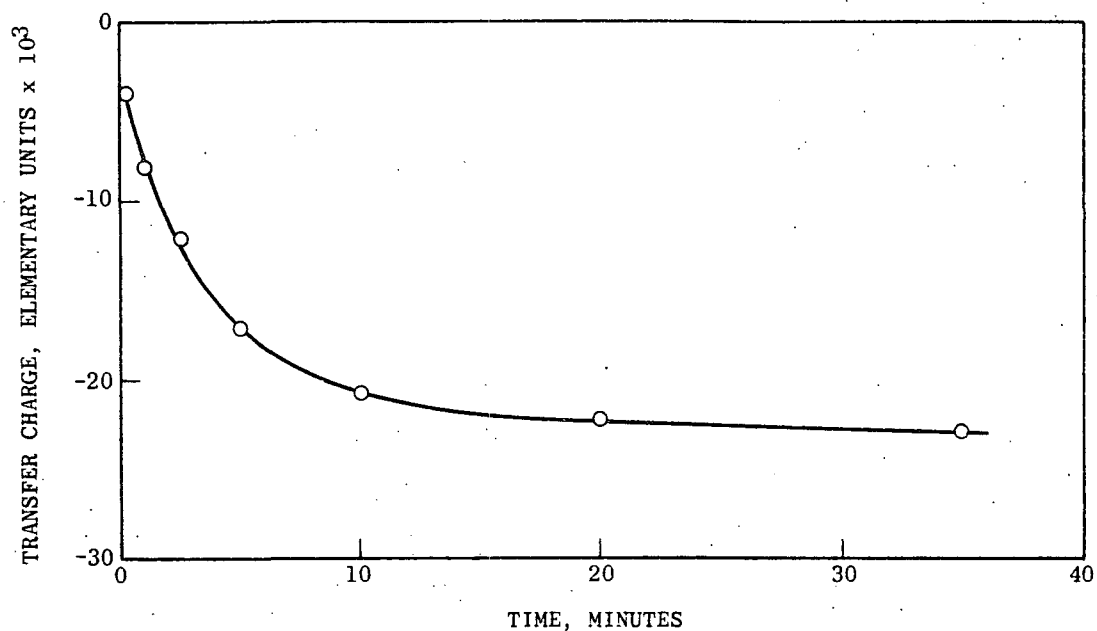


Figure 25. Time dependence of transfer charge from 3.5  $\mu\text{m}$  NaCl particles with a precharge of -6060 elementary charges to a platinum probe cleaned with alcohol-water.

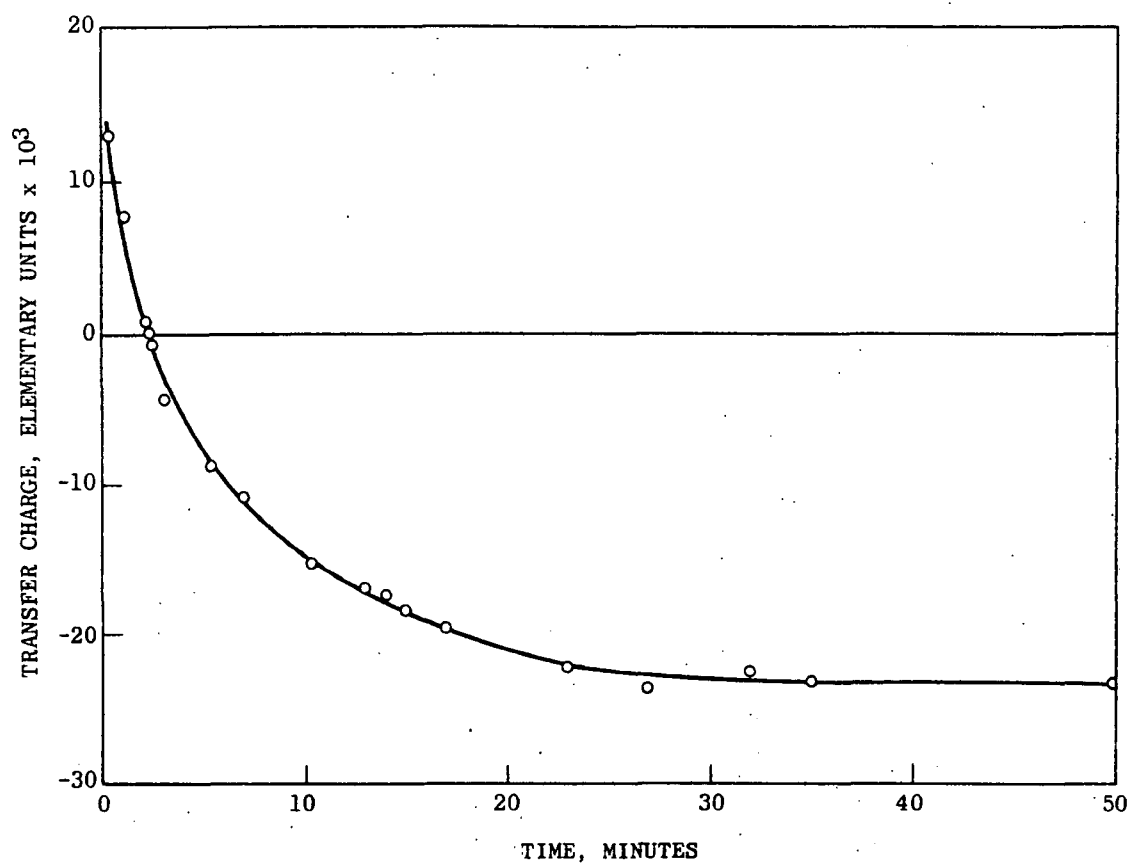


Figure 26. Same as Figure 25 except that the precharge was -6400 elementary charges and the probe was first exposed to potassium biphthalate aerosol.

TABLE 5. CHARGE TRANSFER FOR PARTICLE VELOCITY 75 m/s

Particle	Probe	Transfer charge/Precharge		
		Precharge > 0	Precharge < 0	Average
Methylene Blue	Stainless steel	0.026	0.068	0.047
" "	Stainless steel	0.031	0.031	0.031
" "	Inconel	0.041	0.041	0.041
" "	Titanium	0.030	0.053	0.042
" "	Platinum	0.039	0.072	0.056
Potassium Bi-phthalate	Stainless steel	0.022	0.022	0.022
" "	Inconel	0.023	0.055	0.039
" "	Inconel	0.067	0.063	0.065
" "	Titanium	0.024	0.031	0.028
" "	Titanium	0.023	0.023	0.023
" "	Platinum	0.016	0.060	0.038
Sodium Chloride	Inconel	0.56	0.20	0.38
" "	Titanium	0.47	0.24	0.36
" "	Titanium	0.60	0.30	0.45
" "	Platinum	0.32	0.55	0.44
" "	Platinum	0.32	0.62	0.47

the probe material. The fraction of precharge transferred by methylene blue averaged over all probe materials is  $0.043 \pm 0.009$ ; the corresponding value for potassium biphthalate is  $0.036 \pm 0.016$ . The errors quoted are the standard deviations computed from the data. Since the values for the two particle materials are not significantly different, we form the overall average for methylene blue, potassium biphthalate and all probe materials obtaining  $0.039 \pm 0.013$ . On the other hand the fraction of precharge transferred by sodium chloride averaged over all probe materials is  $0.42 \pm 0.05$ . This is an order-of-magnitude larger and in fact represents a large fraction of the total precharge. The implication is that the sodium chloride is more conducting than the methylene blue and potassium biphthalate, probably due to residual moisture in spite of the low relative humidity ( $< 5\%$ ) of the dilution air used to dry the particles.

## SECTION 5

### EXPERIMENTS WITH A FLUIDIZED BED AEROSOL GENERATOR

#### THE FLUIDIZED BED

A separate series of measurements were performed with aerosol generated by a fluidized bed. The object of this work was to produce aerosol particles for investigations of contact charging with insoluble materials, including metals, which cannot be used in the vibrating orifice aerosol generator.

The fluidized bed affords a method of generating aerosols from a powder or dust sample. (14) The principal problem encountered in producing such an aerosol is agglomeration of the particles which adhere to each other with very strong forces. The fluidized bed aerosol generator consists of a bed of large particles suspended in a fluidized state by an upward flow of gas. A powder sample of smaller particles is added to the bed. The smaller particles become attached to the bed particles and are dispersed throughout the bed. During bed particle collisions, individual powder particles may be dislodged and become entrained in the gas flow, emerging from the bed to form an aerosol.

Figure 27 is a drawing of the fluidized bed which was machined from stainless steel and chromium plated for abrasion resistance. The powder is fed into the bed by a Teflon screw driven by a stepping motor. The rotation rate is controlled by the pulse frequency from the electronic motor drive circuit.

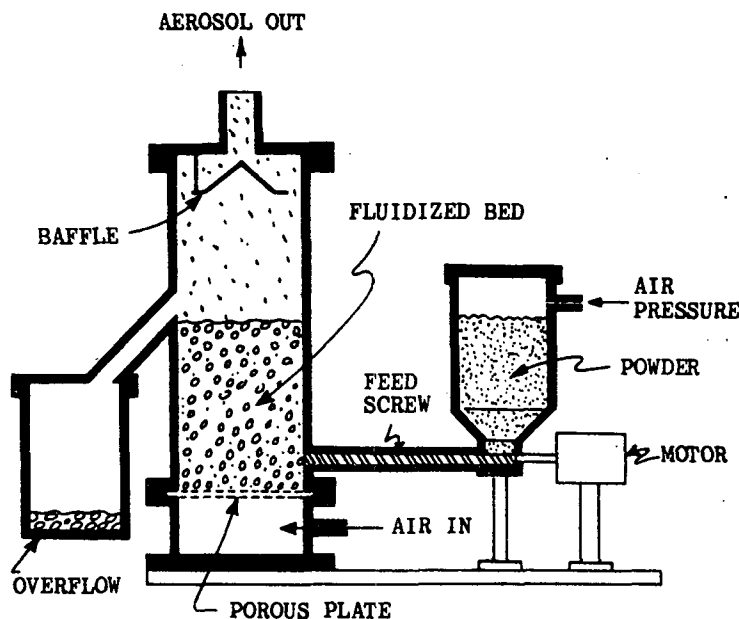


Figure 27. Fluidized Bed Aerosol Generator

Several versions of the feed screw were tried before one was found which functioned. The problem is sticking of the feed screw caused by the powder. The best results were obtained with a loose fitting feed screw and by applying air pressure on the powder container.

Clean air enters the bed via the plenum at the bottom. A porous plate of sintered stainless steel is clamped between the bottom plenum and the upper cylinder. The sintered plate supports the 150  $\mu\text{m}$  nickel bed particles which initially filled the space up to the overflow tube. The conical baffle at the top is designed to prevent bed particles from leaving the cylinder.

As the air flow rate was increased, the pressure drop across the bed as measured with a manometer increased linearly until a break point was reached at about 24.5 LPM, indicating the onset of fluidization (Figure 28). An operating flow rate of 30 LPM was chosen. At this flow rate, the bed has expanded approximately 10% vertically and the top surface resembles that of a gently boiling liquid with bubbles rising to the surface.

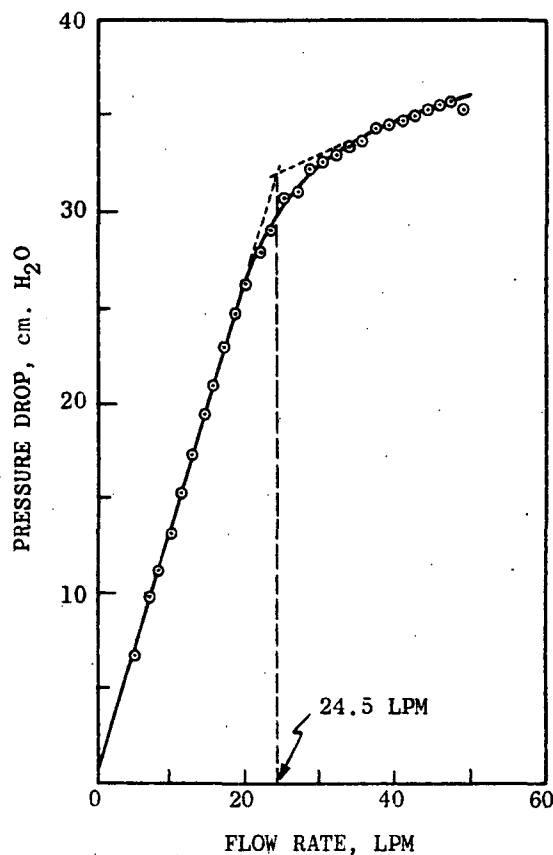


Figure 28.

Pressure drop across the fluidized bed as a function of air flow rate. The break in the curve at 24.5 l/min indicates the onset of fluidization.



When the fluidized bed is initially operated with a fresh charge of nickel particles only, a high concentration of small particles (more than  $10^4$  particles per liter with a peak size less than  $0.3\text{ }\mu\text{m}$ ) is observed in the output air. Several days of continuous operation are required to reduce the concentration to a tolerable background level. Examination of filter samples showed that the particles are fragments of the nickel bed particles. Considerable variation in the nickel particle shape has been found in two different batches of powder from the manufacturer (Sherritt-Gordon Mines Limited, Alberta, Canada). One batch contained particles which were relatively smooth and spherical, while a second batch had particles with a more crystalline angular appearance. The second batch produced much more background aerosol.

#### Aluminum Oxide Aerosol

The initial tests of the fluidized bed were conducted with aluminum oxide powder labelled 3.0 micron, 99.98% pure alumina, agglomerate-free by the manufacturer (Adolf Meller Co., Providence, RI). The size distribution observed with the Climet optical counter is shown in Figure 29. The peak is slightly below  $0.5\text{ }\mu\text{m}$  and most of the particles are smaller than  $1\text{ }\mu\text{m}$  in diameter (optical size). According to the manufacturer, the aluminum oxide particles are grown from seed crystals in the alpha form using a high temperature vapor process. The particle size with which the sample is labelled is said to conform to an industry convention for this product. The actual mean particle size is claimed to be about  $1.5\text{ }\mu\text{m}$ . Examined under a microscope, the powder appears to consist of aggregates of small crystals which are individually a few tenths of a micrometer in diameter. It is not possible to decide whether the particles are loosely aggregated or strongly bonded on the basis of microscopic examination. However, since aluminum oxide is an extremely hard substance, individual crystals will probably not be broken by nickel collisions in the fluidized bed. The observations can be explained by assuming that the powder is deagglomerated in the fluidized bed and that the actual mean particle size is considerably smaller than determined by the manufacturer.

Unfortunately, the aluminum oxide particles produced were too small for use in the contact charging experiment since the impaction probe has a 50% particle size cutoff at  $0.6\text{ }\mu\text{m}$  (aerodynamic diameter). The fluidized bed appears to be capable of generating a usable aluminum oxide aerosol if a properly sized powder sample could be obtained. The scarcity of suitable powder samples appears to be one of the principal difficulties in using the fluidized bed as an aerosol generator.

#### Aluminum Aerosol

Samples of aluminum particles were obtained through the courtesy of the Alcan Aluminum Corporation, Albany, CA. Produced by atomizing from the melt, the particles are spherical. The aluminum is 99.5% pure, with Si (0.2%) and Fe (0.2%) the principal impurities. The material contains traces of Ni, Cu and Mn with some  $\text{Al}_2\text{O}_3$  also present. Most of our measurements were made with sample X-71 which has a narrow size distribution peaking at  $3\text{ }\mu\text{m}$ , according to the manufacturer's measurement with a Coulter Counter. However, our own measurements made with a microscope (Figure 30) show a broad size distribution peaking below  $1\text{ }\mu\text{m}$ .

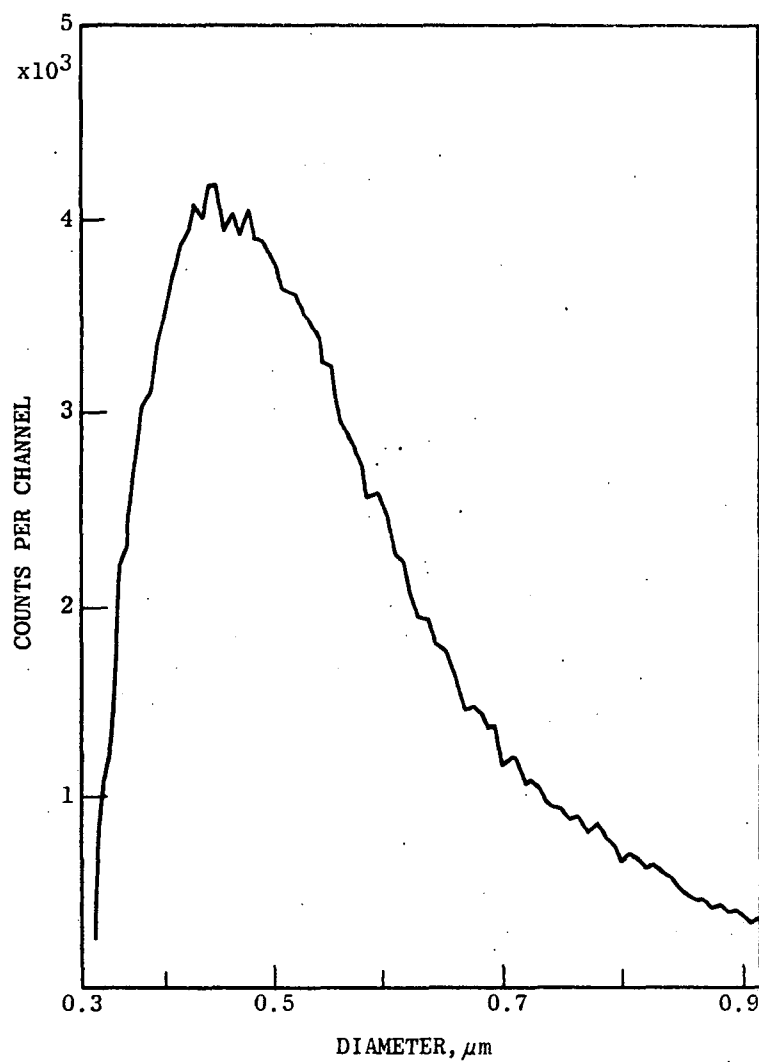


Figure 29. Size distribution of aluminum oxide particles from the fluidized bed aerosol generator.

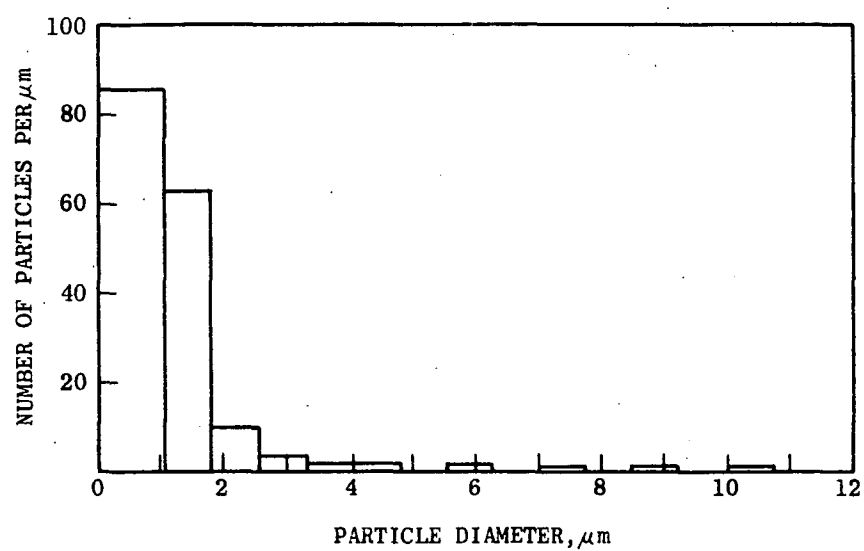


Figure 30. Size distribution of the aluminum particles in the powder sample before it was placed in the fluidized bed.

A few grams of aluminum powder were added to the fluidized bed and the concentration monitored with the optical counter as a function of time after startup. As shown in Figure 31, the concentration falls off rapidly at first and more slowly as time progresses. The initial concentration is so high that a single charge of fresh powder can be used for several hours without running the feed screw.

The size distribution of the Al aerosol measured with the optical counter is shown in Figure 32. This result was surprising since it has no resemblance to the initial size distribution of the powder (Figure 30). The size distribution of the aerosol has a fairly narrow peak. Moreover, the peak position was relatively constant over a period of 5 hours (Figure 33). In the first 30 minutes, the mean particle size decreased by 20% to 40%. Thereafter, the mean size was observed to increase or decrease only slightly, depending on the run.

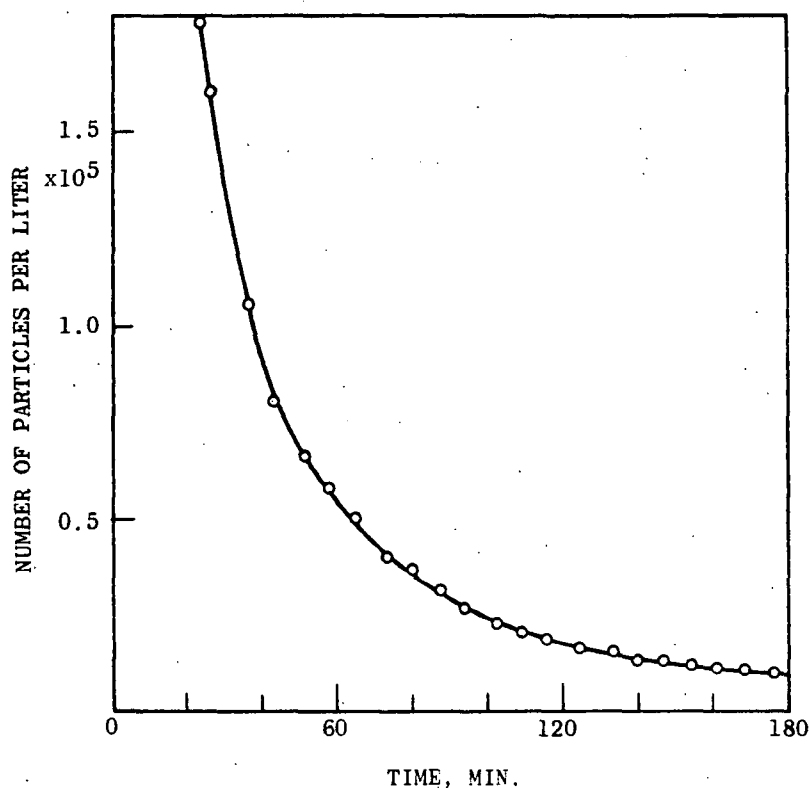


Figure 31

Figure 31. Concentration of aluminum aerosol from the fluidized bed as a function of time after the aluminum was added to the bed.

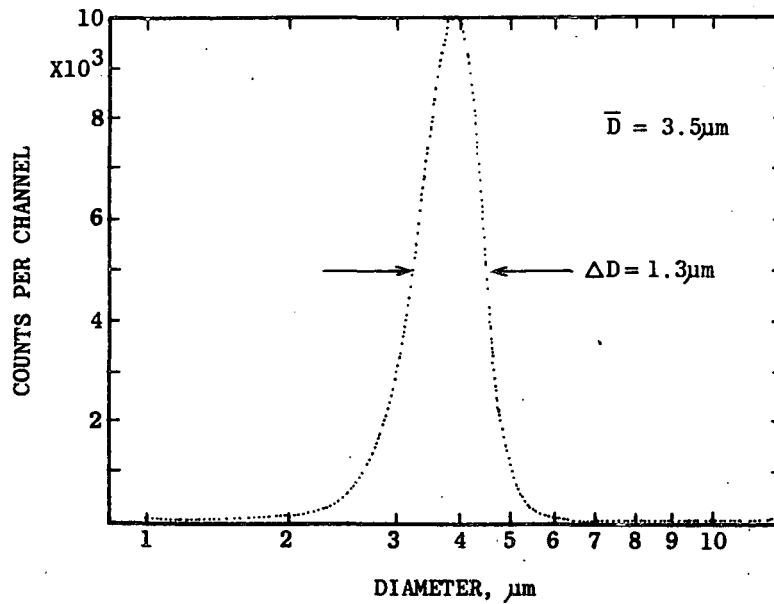


Figure 32. Size distribution of aluminum particles generated by fluidized bed, measured with the optical particle counter.

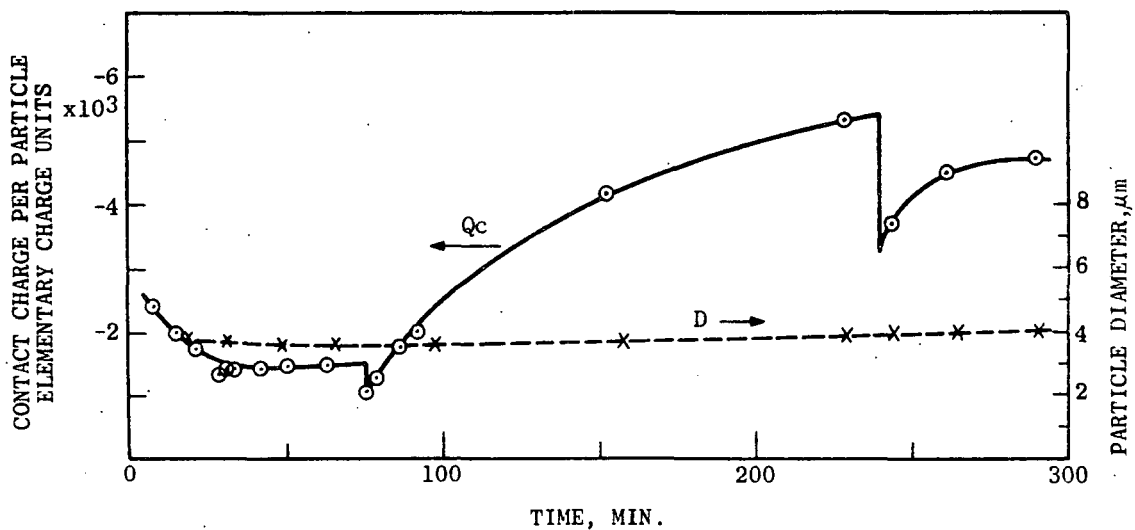


Figure 33. Variation of contact charge and mean particle diameter with time for aluminum aerosol from the fluidized bed. The air flow through the bed was interrupted at 76 minutes and 240 minutes. The increase of contact charge with a long time constant is attributed to increased conductivity of the surfaces of the aluminum particles due to grinding in the fluidized bed.

A sample of the aluminum aerosol was taken on a Nuclepore filter. Examination of the sample under an optical microscope revealed a surprise--the aluminum particles were disk-shaped. The particles were subsequently studied with the higher resolution afforded by a scanning electron microscope. The elemental composition of the particles was checked by x-ray fluorescence. The aluminum powder used to generate the aerosol was found to be initially spherical with a wide range of particle size.

The aluminum particles on the Nuclepore filter were found to be thin disks with diameters in the 4-6  $\mu\text{m}$  range. The disk shapes were remarkably regular; some of them had scalloped edges. Some large irregular particles were seen which may have been deposited early in the run before stable conditions were established.

The flat shape of the aluminum particles obviously implies that the aluminum is deformed during collisions between the large, hard nickel bed particles. We postulate that the remarkably uniform disk shape and uniform size can be explained by assuming that the circular area of the disks corresponds to the contact area between the nickel particles. We can test this idea quantitatively by applying the Hertz theory of elastic deformation to a collision of two spherical nickel particles with a small aluminum particle between them. We assume that the velocities after impact are zero. (The conclusions are unchanged even if the particles rebounded with nearly their initial velocities.) Taking the diameter of the contact area of the nickel particles to be 4  $\mu\text{m}$ , the initial velocities of the nickel particle are calculated to be 45 cm/sec or 8% of the terminal falling velocity. This seems fairly reasonable. The pressure on the contact area is  $1.1 \times 10^{10}$  dynes/cm<sup>2</sup>. The yield strength of annealed aluminum ranges from  $1.22 \times 10^8$  dynes/cm<sup>2</sup> (99.996% Al) to  $3.45 \times 10^8$  dynes/cm<sup>2</sup> (99.0% Al). Therefore, the calculated pressure exceeds the yield strength by a factor 30 or more. We conclude that the postulated model of the disk formation process is quantitatively consistent with the observations. Evidently, the aluminum is worked on during the collisions, small particles are amalgamated and large particles broken up so that the emergent aerosol particles have a size distribution determined by the fluidized bed and not by the aluminum feed material.

#### CHARGE TRANSFER MEASUREMENTS WITH ALUMINUM AEROSOL

Preliminary experiments showed that the aluminum aerosol from the fluidized bed is uncharged. This was a somewhat surprising finding. The background nickel aerosol observed during the clean-up phase of the fluidized bed gives a positive contact current to the stainless steel probe. As a precaution for subsequent work the Kr-85 neutralizer was placed just before the impaction probe.

The contact charge observed from the aluminum aerosol (Sample X-71) and a stainless steel probe is shown in Figure 33. The decrease during the first 30 minutes is probably related to the decrease in mean particle size during that time and possibly to changes in particle shape. Subsequently, the contact charge increases, approaching an asymptotic value. The air flow in the bed was interrupted briefly at 76 minutes and 240 minutes. The contact charge dropped sharply, and then increased rapidly following start-up. These observations can be explained by assuming that the aluminum particles are

coated with an oxide layer. In operation, the working of the aluminum brings fresh metal to the surface. The higher conductivity increases the observed contact charge. Evidently the oxidation is a rapid process, affecting the contact charge after only a few minutes of interruption. The magnitude of the asymptotic contact charge is about 10,000 elementary charges, much larger than that obtained for insulating materials. These results agree with the dependence of the contact charge on resistivity observed previously by John. (9)

The transfer of induced charge was also observed. Because the particles are initially uncharged, a new method was devised to charge the particles by induction, namely, by placing a positive potential on the slit which is opposite the grounded impaction probe. The particles then contact the probe in the presence of an electric field which superimposes an induced charge on the contact charge. When the induction voltage is varied, a charge transfer curve is observed as shown in Figure 34. The straight line shows that the oxide layer is not thick enough to cause a rectifying action. Although the data for Figure 34 were taken after the bed had operated for about 200 minutes, data taken for earlier times also yielded linear charge transfer curves.

Data on the contact charge from another run is shown in Figure 35. The bed had been previously run, therefore the time shown is after restart, and the charge increases immediately in agreement with the previous data. For comparison,  $\beta$ , the slope of the charge transfer curve, is plotted in Figure 36. This shows that  $\beta$  also increases with running time but it does not approach the asymptotic value as rapidly as  $Q_c$ . In our previous work with insulators (particles from the vibrating orifice aerosol generator) we observed that  $Q_c$  was less sensitive to the surface condition of the probe than was  $\beta$ . The present observations are similar, except that the oxide layer is on the particles rather than the probe.

Figure 37 summarizes measurements made with a different sample of aluminum powder. From an unknown supplier, the particles were large and irregular in shape but smooth as though derived from a molten state. Although this aluminum feed material was quite different, the particles produced by the fluidized bed were closely similar to those previously observed, and the charge measurements showed qualitatively similar behavior.

Finally, the contact charge was measured as a function of the flow rate of the air in the impactor (Figure 38), using the X-17 aluminum. Because  $Q_c$  increases with time, the measurements were cycled from low flow rates to high and back down. Within the errors the data are again in agreement with a linear dependence of  $Q_c$  on particle impact velocity.

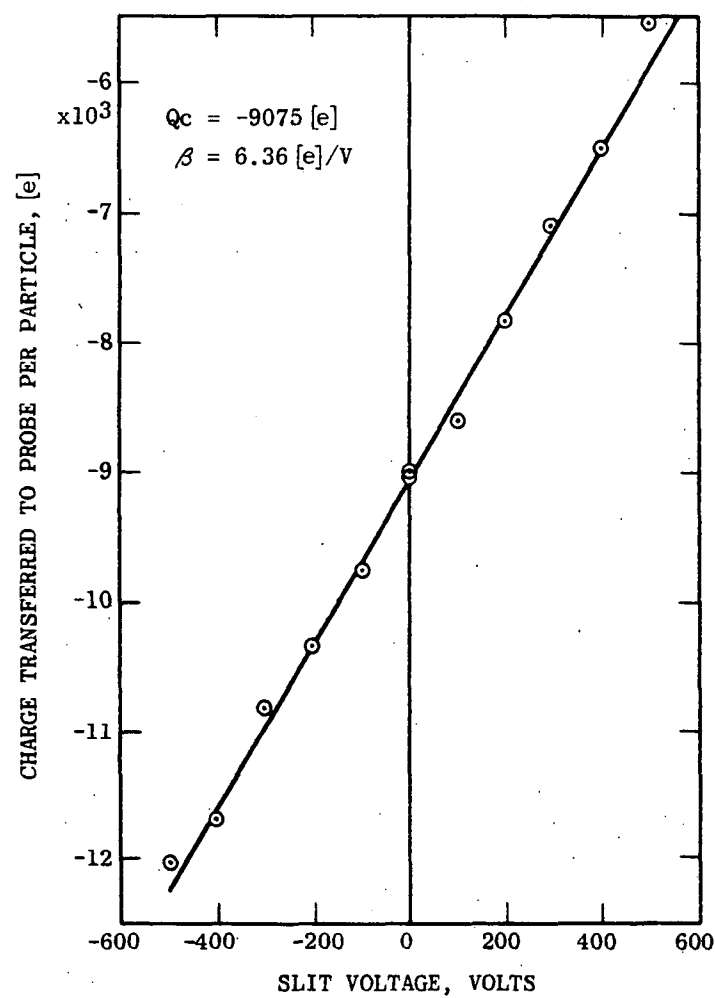


Figure 34. Charge transferred from aluminum particles to a stainless steel probe as a function of induction voltage.



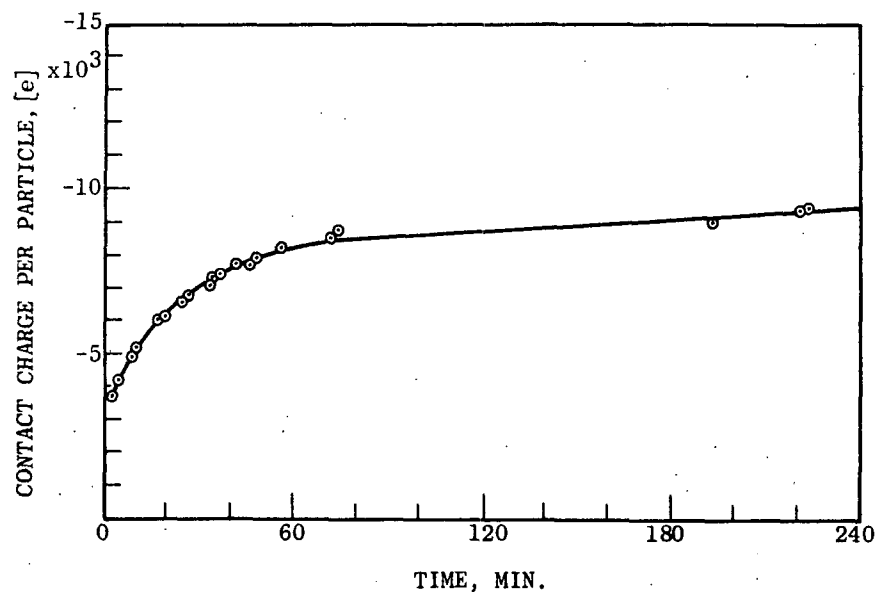


Figure 35. Contact charge for aluminum particles on stainless steel vs. time after restart of the fluidized bed showing a rapid initial rise.

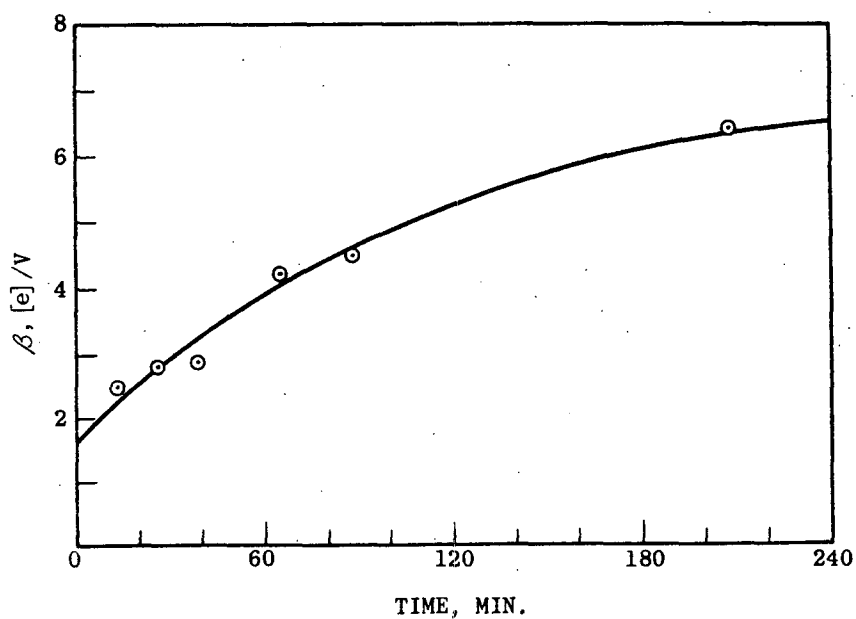


Figure 36. Slope of the charge transfer curve,  $\beta$ , vs. time for the same run as Figure 35.

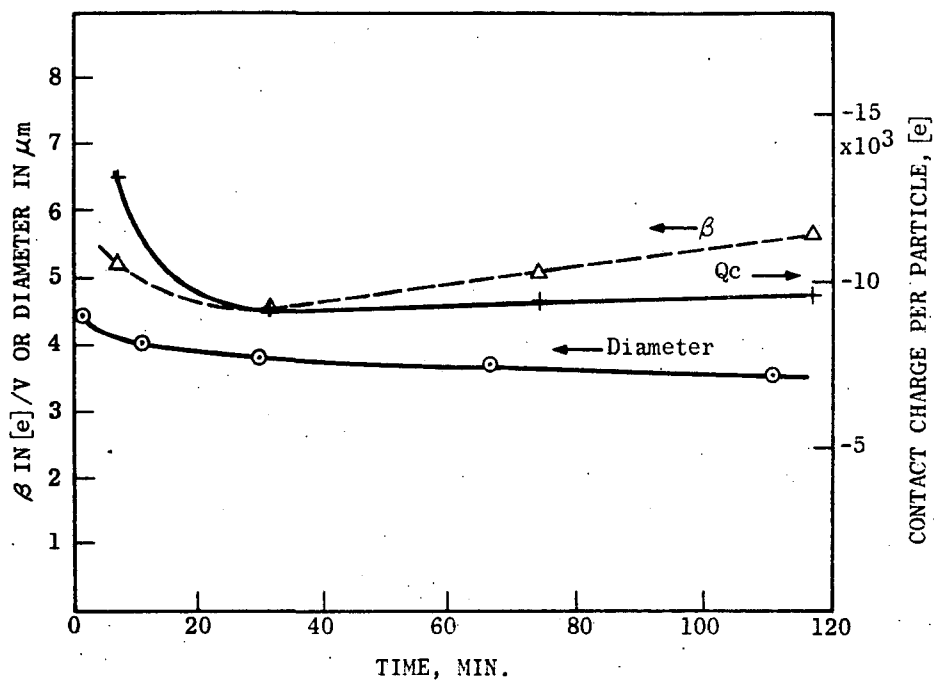


Figure 37. Particle size, contact charge and slope of the charge transfer curve vs. time for a different aluminum feed material than shown in the previous figures.

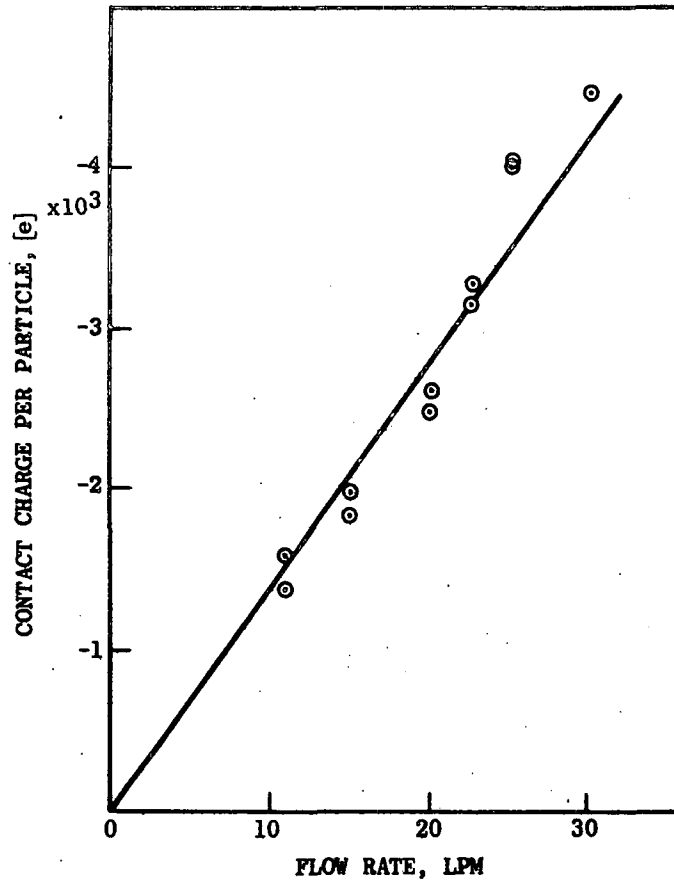


Figure 38. Contact charge of aluminum vs. air flow rate in the impaction probe.

## SECTION 6

### THEORY OF CHARGE TRANSFER

#### MODEL OF CHARGE TRANSFER PROCESS

The origins of the model to be considered here are in the work by Cheng and Soo (15) who pointed out that the charge transfer is a dynamic process. An elastic sphere impacting on a surface will be deformed, a circular contact area being established during the impact, as illustrated in Figure 39. Cheng and Soo calculated the charging of the capacity of the sphere by the contact potential. Later, Cole, et al., (16) considered that the relevant capacity is formed by the circular contact area and the effective separation of the surfaces. Masuda, et al., (17) employed this model with an additional factor to account for the incomplete charging of the capacity owing to the resistance of the material. Both Cole, et al., and Masuda, et al., included additional effects which we do not retain here. It will be shown that one of the effects is negligible. The other effects are complications from multiple bounces or space charge which are not present here. We will selectively develop here those parts of the theory which we believe to be applicable. In fact, the unique data presented here allows the first direct test of the theory for single impacts of monodisperse particles of known uniform charge.

#### Theory of Elastic Impact

When a sphere impacts on a plane surface, it can be shown from the elasticity theory of Hertz that the contact area,  $A$ , and the duration of the impact,  $\Delta t$ , will be given by (18):

$$(1) \quad A = \pi a^2 \alpha$$

$$(2) \quad \Delta t = \frac{2.94}{v} \alpha a$$

$$\text{where } \alpha = \left[ \frac{5}{4} \pi^2 \rho v^2 (k + k_s) \right]^{2/5}$$

$a$  = particle radius

$v$  = particle velocity

$\rho$  = particle density

$k$  = elasticity parameter for particle material

$k_s$  = elasticity parameter for surface material

In obtaining the above expression for  $\alpha$  we have taken the rebound coefficient to be one, the impact angle  $\theta = \frac{\pi}{2}$ , and the surface radius and mass to be infinite.

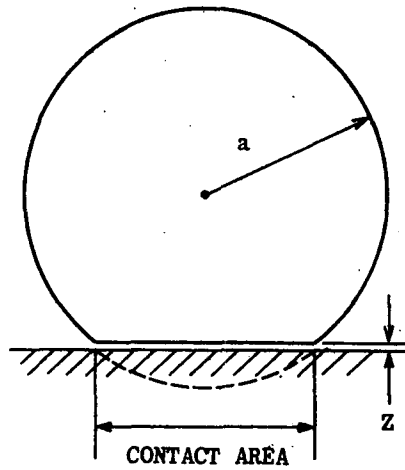


Figure 39. Illustration of the contact area and separation distance  $Z$  during the impaction of an elastic sphere with a surface.

The elasticity parameter  $k$  is defined by

$$k = \frac{1 - \nu^2}{\pi E}$$

where  $\nu$  = Poisson's Ratio ( = 0.3 for most materials)

$E$  = Young's Modulus

### Transfer of Precharge from Insulating Particles

The duration of the impact is quite short, as can be seen by estimating  $\Delta t$  for methylene blue or potassium biphthalate particles impacting on a metal probe. We take  $a = 1.5 \mu\text{m}$ ,  $v = 75 \text{ m/s}$ ,  $k = 9 \cdot 10^{-11} \frac{\text{m}^2}{\text{N}}$ ,  $k_s = 1.5 \cdot 10^{-12} \frac{\text{m}^2}{\text{N}}$ .

Then equation (2) gives  $\Delta t = 10^{-8}$  sec. Since  $\Delta t$  is small and the particle is an insulator, only the precharge within the Hertz contact area is transferred. We further assume that the precharge is on the surface of the particle and the charge within the contact area is completely transferred. The ratio of the charge transferred,  $Q_t$ , to the precharge on the particle,  $Q_0$ , is given by:

$$\begin{aligned} \frac{Q_t}{Q_0} &= \frac{A}{4\pi a^2} \\ &= \frac{\alpha}{4} \\ (3) \quad \frac{Q_t}{Q_0} &= \frac{1}{4} \left[ \frac{5}{4} \pi^2 \rho v^2 (k + k_s) \right] \frac{2}{5} \end{aligned}$$

Equation (3) predicts that the fraction of precharge transferred is independent of particle radius, as we observe experimentally.

In order to test equation (3) quantitatively the elastic constant  $k$  is needed. Since  $k$  is unknown for methylene blue and potassium biphthalate, we estimate that  $k$  is in the range spanned by that for ionic crystals like NaCl and plastics like polystyrene, i.e., from  $3 \cdot 10^{-11}$  to  $9 \cdot 10^{-11} \frac{\text{m}^2}{\text{N}}$ .

Then taking  $a = 3 \mu\text{m}$ ,  $v = 75 \text{ m/s}$ ,  $k_s = 1.5 \cdot 10^{-12} \frac{\text{m}^2}{\text{N}}$  (steel)

$$\frac{Q_t}{Q_0} = 0.024 \text{ to } 0.037$$

where the spread corresponds to the range in estimated  $k$ . This is to be compared to the experimental average value,  $0.039 \pm 0.013$ , for methylene blue and potassium biphthalate particles impacting on stainless steel, Inconel, titanium and platinum. The agreement is very good for the larger value of  $k$ . If  $k$  is actually near the lower value, the additional charge transfer observed experimentally could be explained by surface conduction from a small distance outside the contact area. It would be necessary to assume conduction from a distance only 25% larger than the radius of the contact area.

In the above discussion we have assumed complete transfer of the charge in the contact area. However, the experimental data shows that for some materials the fraction of precharge transferred is somewhat greater for positive precharge than for negative precharge. In these cases, the contact charge is always positive. When the contact charge is negative the dependence on the sign of the precharge is reversed. This effect can be interpreted in terms of a weakly rectifying p-n junction (19) formed at the particle-probe contact. For positive contact charge, the particle surface material is p-type, the probe surface material n-type. When neutral particles contact the probe, electrons flow from the probe to the particle and positive charge (holes) flow from the particle to the probe until the contact potential is established. If the particle carries a positive precharge, this produces a positive bias voltage across the junction, increasing the charge transfer rate. On the other hand negative precharge will impede the charge transfer. For negative contact charge the effects are reversed. The rectifying action is considered to be weak because the slopes of the transfer curves are not greatly different with change of sign of precharge and the curves are linear.

Figures 23-26 show that the charge transferred varies with time. The effect was observed with all particle and probe combinations. We can show that the time dependence is consistent with the assumption that the charge transfer characteristics of the probe surface are altered by contact with particles. We must calculate the rate at which the probe surface is covered by Hertz contact circles whose centers are randomly located. The result is

$$(4) \quad b = 1 - e^{-\frac{t}{T}}$$

where  $b$  = fraction of probe surface contacted

$t$  = time of exposure to aerosol

$T$  = time constant

The time constant is given by

$$T = \frac{S}{nA}$$

with  $S$  = total area of probe surface

$n$  = number of particles incident per unit time

$A$  = Hertz contact area of a particle

Taking parameter values from our experiments,  $n = 10^4$  particles/s,  $a = 1.5 \mu\text{m}$ ,  $A = 0.03 (4\pi a^2)$ ,  $S = 0.04 \text{ cm}^2$ , we obtain  $T = 8$  minutes.

This is a quite reasonable estimate. Since microscopic examination revealed that very few particles stick to the surface, we must assume that the changes produced by contact originate in transfer of minute amounts of material and, possibly, some mechanical alterations from the impact. The high sensitivity to surface impurities again suggests semiconductor effects.

For NaCl,  $\frac{Q_t}{Q_0}$  ranged from 0.2 to 0.6. This large fractional charge transfer probably results from surface conduction produced by adsorbed moisture.

### Contact Charge

A parallel plate capacitor is formed by the Hertz contact area and the separation of the particle and probe surfaces. The separation of the surfaces will be somewhat larger than the range of repulsive molecular forces owing to surface irregularities. (16) These irregularities also mean that the entire Hertz area is not in molecular contact. However, the unknown surface topography can be included in an equivalent "effective" separation  $z$ . In the following,  $z$ , will be set equal to  $10^{-9}\text{m}$  (10 Å) which is probably correct within an order of magnitude. (20)

The contact charge,  $Q_c$ , will be given as a function of time by:

$$(5) \quad Q_c = CV_c (1 - e^{-\frac{\Delta t}{\tau}})$$

where  $C$  is the electrical capacity and  $\tau$  is the charge relaxation time of the particle material.  $V_c$  is the contact potential between the particle and probe materials. (The probe material will always be taken to be a metal). The capacity  $C = \frac{\epsilon_0 A}{z}$ , and  $A$  is given by equation (1).

Therefore

$$(6) \quad Q_c = \frac{\pi \epsilon_0 V_c}{z} \left[ \frac{5}{4} \pi^2 \rho v^2 (k + k_s) \right]^{\frac{2}{5}} a^2 (1 - e^{-\frac{\Delta t}{\tau}}) \quad (\text{for all materials})$$

### Contact Charge for Conductors--

When the particle material is a metal,  $\Delta t \gg \tau$ , and the charging will be complete:

$$(7) \quad Q_c = \frac{\pi \epsilon_0 V_c}{z} \left[ \frac{5}{4} \pi^2 \rho (k + k_s) \right]^{\frac{2}{5}} v^{\frac{4}{5}} a^2 \quad (\text{for conductors})$$

This equation predicts that for conductors,  $Q_c$  is proportional to  $v^{\frac{4}{5}}$  and  $a^2$ . No data is available on the dependence of  $Q_c$  on particle radius in the case of conductors. A comparison to the theory is partially afforded by the NaCl data. As previously noted, the large fraction of precharge transferred by NaCl particles indicates the presence of surface conductivity. In addition,  $Q_c$  for NaCl was proportional to  $a^{(2.45 \pm 0.14)}$ . The exponent was lower than the average value of  $3.04 \pm 0.08$  for the insulating particles. (It will be shown below that the theory predicts an exponent of 3 for insulators). Thus the NaCl particles, which are partially conducting, also yield a value of the exponent intermediate between the prediction for conductors and insulators.

The predicted dependence of  $Q_c$  on  $v^{0.8}$  is to be compared to the measured dependence on  $v^{1.0}$  for aluminum particles. This is already fair agreement. It is probable that  $z$ , the effective particle-surface spacing will decrease as the velocity increases. This would increase the velocity exponent, bringing the theory closer to experiment. However, the change in  $z$  cannot be predicted theoretically.



We evaluate equation (7) for aluminum particles impacting on steel and the following parameters:  $a = 1.5 \mu\text{m}$ ,  $V_c = 1 \text{ V}$ ,  $v = 75 \text{ m/s}$ ,  $z = 10^{-9} \text{ m}$ . The result is  $Q_c = 2 \cdot 10^4$  elementary charges. This compares favorably to the measured value of  $1 \cdot 10^4$  elementary charges for (non-spherical) aluminum particles. The agreement is well within the uncertainty in the values to be used for  $z$  and  $V_c$  which require a detailed knowledge of the surface for accurate evaluation.

It is necessary to discuss why the contact charge does not depend on the magnitude of the precharge. This is an experimental fact implied by the observed linearity of the charge transfer curves. The precharge on the surface of the particle produces a potential  $V_Q$ , at the contact point which tends to transfer charge. In computing  $V_Q$ , the effect of the image charge in the metal surface of the probe must be taken into account. The result is (16)

$$(8) \quad V_Q = \frac{Q_0 z}{2\pi a^2 \epsilon_0}$$

Evaluating this expression for  $z = 10^{-9} \text{ m}$ ,  $a = 1.5 \mu\text{m}$  and  $Q_0 = 10^3$  elementary charges,

$$V_Q = 1 \cdot 10^{-3} \text{ volt}$$

Since  $V_c$  is of the order of 1 volt,  $V_Q$  can be neglected.

Contact Charge for Insulators--

For particles of insulating materials,  $\tau \gg \Delta t$ , and

$$\begin{aligned} Q_c &= C V_c \cdot \frac{\Delta t}{\tau} \\ &= \frac{\epsilon_0 A}{z} \cdot V_c \cdot \frac{\Delta t}{\tau} \end{aligned}$$

The relaxation time  $\tau$  is given by (21)

$$\tau = K \epsilon_0 \rho_p$$

with  $K$  = dielectric constant

$$\rho_p = \text{resistivity}$$

Finally,

$$(9) \quad Q_c = \frac{2.94 \pi V_c}{z K \rho_p} \left[ \frac{5}{4} \pi^2 \rho (k + k_s) \right]^{\frac{4}{5}} v^{\frac{3}{5}} a^3 \text{ (for insulators)}$$

This equation predicts that for insulators,  $Q_c$  is proportional to  $a^3$  as was experimentally observed.  $Q_c$  is also predicted to be proportional to  $v^{0.6}$  whereas experimentally  $Q_c$  is proportional to  $v^{1.0}$ . As discussed above for conductors, the agreement with theory would be better if the change of  $z$  with velocity were taken into account. On the other hand we note that the velocity dependences for conductors and insulators are predicted to be  $v^{0.8}$  and  $v^{0.6}$  respectively, whereas both are measured to be  $v^{1.0}$ .

To calculate  $Q_c$  from equation (9) the resistivity  $\rho_p$  must be known. In practice  $\rho_p$  is not known and the possible range of resistivities is enormous. Therefore we will reverse the procedure, calculating  $\rho_p$  from the observed  $Q_c$ . For methylene blue and potassium biphthalate, the average  $Q_c$  for particles with 1.5  $\mu\text{m}$  radius was approximately 700 elementary charges. We further take  $V_c = 1$  volt,  $z = 10^{-9}\text{m}$ ,  $K = 3$ ,  $v = 75$  m/s. The result is  $\rho_p = 6 \cdot 10^4$  ohm $\cdot\text{m}$ . This is an acceptable value for the resistivity since the resulting relaxation time is  $\tau = 2 \cdot 10^{-6}\text{s}$ . Then we obtain

$$\frac{\Delta t}{\tau} = 5 \cdot 10^{-3}$$

Therefore the contact time is much smaller than the charge relaxation time of the material, satisfying the definition of an insulator.

#### DISCUSSION OF THE THEORY

It has been shown that the theoretical model accounts quantitatively for the fraction of precharge transferred and for the dependence of contact charge on particle size. The theoretical dependence of contact charge on particle velocity and resistivity are consistent with experiment and the calculated contact charging is of the right order of magnitude. Thus the model can be used as a guide for future investigations and applications of charge transfer between particles and surfaces.

The principal limitation to the theory is that the contact potential is unknown because the surfaces of the particles and probe are insufficiently characterized even with considerable care in their preparation. The probe polishing procedure developed during this work is a recipe for the preparation of a reproducible surface, but the detailed physical and chemical characteristics of the surface are unknown. Similarly the details of the particle surfaces are unknown, although it may be worth noting that the generation of aerosol particles does produce fresh surfaces. The asymptotic increase of the probe current when the probe is first exposed to aerosol also shows the extreme sensitivity of the charge transfer to contaminants on the surface. Thus future progress in understanding the charge transfer process will require elucidation of the properties of the surfaces involved.

## SECTION 7

### IMPLICATIONS OF THE FINDINGS FOR APPLICATIONS

#### PRINCIPAL FACTORS AFFECTING MONITORING

The experimental and theoretical findings presented above can be used for a critical analysis of the application of contact electrification to monitoring of particulate matter. The principal factors will be discussed separately.

##### Probe Design Consideration

The charge transferred to the probe also depends on the probability that the particle impacts on the probe. The impaction probe design developed for this work ensures that all particles above the impaction cutoff size will impact with essentially 100% probability. It is well known that it is difficult to employ inertial impaction below about 0.5  $\mu\text{m}$  particle diameter. Possibly turbulence could be used to cause small particles to impact; this has not been explored here.

The streamlined probe used in some of the IKOR instruments would appear to be an ineffective design in terms of achieving high sensitivity and detection of small particles. (IKOR has more recently offered a probe designed to cause turbulence.) The tubular pipe design of the Konitest causes multiple particle contacts with the probe. Even for insulators the current will depend on the particle size distribution. Additional uncertainty is introduced by the possibility of sliding particle-probe contacts.

It has been shown that the contact charge is proportional to the particle impact velocity. Thus high velocity is desirable in terms of increased sensitivity as well as the lowered particle cutoff size for impaction. Instack probe designs such as that offered by IKOR raise concern that the stack velocity be sufficiently high and constant.

##### Dependence of Sensitivity on the Physical Properties of the Particulate Material

The finding that the contact charge varies as the cube of the particle diameter in the case of insulators means that the probe current will be proportional to the particle mass flow, independent of particle size. However, for metallic conductors, the contact charge is predicted to vary as the square of the particle diameter. The probe current per unit mass will then vary inversely as the particle diameter. Partial conductors, such as an ionic salt which is not completely dry will exhibit an intermediate behavior. Therefore, in general, the probe current will be independent of the particle size distribution only if all the particles are composed of insulating materials.

The contact charge is strongly dependent on the electrical resistivity of the particle material. Theoretically, the range of contact charge per unit mass corresponding to the range of resistivities of all materials would cover a factor of  $10^{14}$ . In practice, we have observed a range somewhat less than  $10^2$ ,

probably because the particle surfaces are never completely dry and clean. This will also be expected for particles emitted by sources, and the response of the detector will vary considerably, depending on the particle resistivity.

The contact charge depends weakly on the elastic parameters of the materials. The theory predicts a maximum variation of the contact charge by a factor of about 5 from hard materials to plastics.

Complications are introduced by friable materials. It is not possible to predict with confidence what the contact charging will be in the presence of particle breakup. Some breakup was present in our NaCl experiments which did not appear to greatly affect the dependence of the charge transfer on particle size. The large fractional charge transfer has been attributed to surface moisture.

### Probe Surface Condition

Ample evidence has been presented of the strong dependence of the charge transfer to the preparation of the probe surface and its history of exposure to aerosol. The probe preparation procedure which has been presented here yields reproducible charge transfer. This procedure or one which produces equivalent results should be used to obtain reliable monitoring performance. It is clear, however, that the detailed properties of the surface are unknown. Similarly, the properties of the particle surfaces are unknown, so that the contact potential cannot be predicted. Contact charge can be of either sign. For a mixture the net charge transferred is detected. If the composition varies, the net sensitivity can vary. It is desirable that the monitoring instrument indicate the sign of the current as an additional useful datum.

### RECOMMENDATIONS FOR MONITORING PROCEDURES

The following recommendations are based on the findings of the present investigation:

1. Prior to monitoring, the probe surface preparation procedure described above should be used.
2. The probe should be exposed to aerosol from the source until the current reaches the asymptotic value.
3. Sticky material should not be monitored since it will coat the probe and affect the charge transfer.
4. The monitor should not be used to sample material whose composition varies with time since the sensitivity and calibration of the instrument varies with the chemical and physical properties of the material.
5. The monitor must be calibrated for each source. Any change in source conditions will require recalibration.
6. The aerosol should be neutralized because the monitor responds to pre-charge on the particles. The aerosol is likely to become charged as a result of mechanical and electrical processes existing within the source.

7. Gaseous ions should be removed from the aerosol to avoid collecting spurious charge.
8. All parts of the monitoring system contacted by the aerosol should be constructed of metal and grounded to avoid charging effects from particles and gas exposed to surfaces of insulators.

#### OVERALL ASSESSMENT OF THE CONTACT ELECTRIFICATION MONITOR

Contact electrification can be used for monitoring in real time with a short time constant. The current is proportional to the mass flow, but the instrument must be calibrated for each source. Any change in source conditions will require recalibration. Because the response depends on unknown detailed properties of surfaces the calibration cannot be predicted quantitatively in terms of fundamental properties of the material sampled. The instrument furnishes a relative measure of the mass flow. The components of a mixture will contribute to the total current with varying sensitivity, depending mainly on the electrical resistivity of the materials. Because the contact potential can be positive or negative, an increase in the proportion of one constituent of a mixture can cause the magnitude of the total current to increase or decrease. The overall sensitivity will depend on the choice of probe material.

For insulating particles the monitor's response is independent of particle size distribution, provided that the probability of impaction on the probe is also independent of particle size. Partial or good conductors are detected with a sensitivity which increases with decreasing particle size for a given mass emission rate. In practice then, change in particle size distribution will usually require recalibration. There will be a lower particle size cutoff in sensitivity determined by the size dependence of the particle impaction probability.

The principal disadvantages of the monitor derive from the fact that the charge transfer is a surface phenomenon. Care is required in preparing and equilibrating the probe. Loading of the probe will require cleaning at intervals depending on the particular source; it will not be practical to sample some sticky materials. The monitor's performance is vulnerable to subtle changes in the properties of the material sampled.

Within the inherent limitations it would appear that the monitor can be useful for certain types of sources. The instrument is relatively simple and low in cost. The electrical signal is convenient for data processing. Transient events can be monitored which may be useful in detecting malfunctions of emission control devices, etc. The total emission can be determined by a simple integration of the current signal. The output is proportional to gravimetric mass, assuming constant source emission conditions.

## REFERENCES

1. Schutz, A. Eine Anordnung zur Registrierenden Kontaktelektrischen Staubbmessung. Staub 24: No. 9, 359-363, 1964.
2. Schutz, A. A Recording Dust-Measuring Instrument Based on Electric Contact, with Logarithmic Indication. Staub 26: No. 5, 18-22, 1966.
3. Prochazka, R. Neueste Entwicklung des auf Kontaktelektrischer Basis Beruhenden Staubgehaltsmessgerates Konitest. Staub 24: No. 9, 353-359, 1964.
4. Prochazka, R. Recording Dust Measurement with the Konitest. Staub 26: No. 5, 22-28, 1966.
5. Schutz, A. Technical Dust Control Principles and Practice. Staub 26: No. 10, 1-8, 1966.
6. Cheng, L. and S. L. Soo. Charging of Dust Particles by Impact. J. Appl. Phys. 41: 585-591, 1970.
7. IKOR, Inc., unpublished reports, and A. H. Gruber, private communication.
8. Schnitzler, H. Messtand für die Prüfung und Kalibrierung von Registrierenden Staub- und Gasmessgeräten in einem Steinkohlengefeuerten Kraftwerk. Schrreihe Ver. Wass-Boden Lufthyg, Berlin-Dahlem, V. 33, Stuttgart, 1970.
9. John, W. Investigation of Particulate Matter Monitoring Using Contact Electrification. Environmental Protection Agency, Research Triangle Park, NC, Technology Series Report Number EPA-650/2-75-043, February, 1975, 45 pp.
10. Harper, W. R. Contact and Frictional Electrification. Oxford U. Press, Oxford, 1967, 369 pp.
11. John W. Contact Electrification Applied to Particulate Matter-Monitoring. In: Fine Particles, Aerosol Generation, Measurement, Sampling and Analysis, B.Y.H. Liu, ed., Academic Press, NY, 1976, pp 649-667.
12. Berglund, R. N. and B.Y.H. Liu. Generation of Monodisperse Aerosol Standards. Envir. Sci. and Tech. 7:147-153, 1973.
13. Reischl, G., W. John and W. Devor. Uniform Electrical Charging of Monodisperse Aerosols. J. Aerosol Sci. 8:55-65, 1977.
14. Guichard, J. C. Aerosol Generation Using Fluidized Beds. In: Fine Particles, Aerosol Generation, Measurement. Sampling and Analysis, B.Y.H. Liu, ed., Academic Press, NY, 1976, pp. 173-193.

15. Cheng, L. and S. L. Soo. J. Appl. Phys. 41: 585-591, 1970.
16. Cole, B. N., M. R. Baum and F. R. Mobbs. An Investigation of Electrostatic Charging Effects in High-Speed Gas-Solids Pipe Flows. Proc. Instn. Mech. Engrs. 184, Pt 3C: 77-83, 1969-70.
17. Masuda, H., T. Komatsu and K. Iinoya. The Static Electrification of Particles in Gas-Solids Pipe Flow. Unpublished manuscript, Kyoto Univ., Kyoto, Japan.
18. Soo, S. L. Dynamics of Charged Suspensions. In: Topics in Current Aerosol Research, Vol. 2, International Reviews in Aerosol Physics and Chemistry. Pergamon Press Ltd., Oxford, 1971, p. 71.
19. Malmstadt, H. V., C. G. Enke, S. R. Crouch and G. Horlick. Electronic Measurements for Scientists. W. A. Benjamin, Inc., Menlo Park, CA, 1974, pp. 207-208.
20. Dahneke, B. The Influence of Flattening on the Adhesion of Particles. J. Colloid and Interface Sci. 40: 1-13, 1972.
21. Hendricks, C. D. Introduction to Electrostatics. In: Electrostatics and Its Applications, A. D. Moore, ed. John Wiley and Sons, NY, 1973, p. 26.

TECHNICAL REPORT DATA (Please read Instructions on the reverse before completing)		
1. REPORT NO. EPA-600/2-78-212	2.	3. RECIPIENT'S ACCESSION NO.
4. TITLE AND SUBTITLE INVESTIGATION OF PARTICULATE MATTER MONITORING USING CONTACT ELECTRICITY Final Report	5. REPORT DATE October 1978	
	6. PERFORMING ORGANIZATION CODE	
7. AUTHOR(S) Walter John, Georg Reischl, William Devor, and Jerome J. Weslowski	8. PERFORMING ORGANIZATION REPORT NO.	
9. PERFORMING ORGANIZATION NAME AND ADDRESS Air and Industrial Hygiene Laboratory California Department of Health 2151 Berkeley Way Berkeley, California 94704	10. PROGRAM ELEMENT NO. 1AD712 BA-04 (FY-77)	
	11. CONTRACT/GRANT NO. R 803719-01-2	
12. SPONSORING AGENCY NAME AND ADDRESS Environmental Sciences Research Laboratory - RTP, NC Office of Research and Development U.S. Environmental Protection Agency Research Triangle Park, N. C. 27711	13. TYPE OF REPORT AND PERIOD COVERED Final	
	14. SPONSORING AGENCY CODE EPA/600/09	
15. SUPPLEMENTARY NOTES Previous Report: EPA-650/2-75-043, February 1975		
16. ABSTRACT To better understand the contact electrification monitor for particulate matter, charge transfer by aerosol particles impacting on metal surfaces has been investigated. Mono-disperse, uniformly charged or neutral aerosol particles (1-5 $\mu$ m diameter) from a vibrating orifice or fluidized bed generator were bounced on a metal probe. The transfer of precharge from the particles was found to be a sensitive indicator of the probe surface condition. A surface preparation procedure was developed which yielded linear charge transfer curves.  Measurements were made of methylene blue, potassium biphthalate, sodium chloride and aluminum particles impacting on stainless steel, Inconel, titanium, and platinum probes. For insulating materials, the transfer of precharge was independent of particle size while the contact charge was proportional to the cube of particle diameter and directly proportional to impact velocity. The magnitude of the contact charge was strongly dependent on the electrical resistivity of the material. A theoretical model was found to account semi-quantitatively for all aspects of the data. A major remaining difficulty is the lack of knowledge of the contact potential. The implications of these findings for monitoring applications are discussed in detail and the advantages and disadvantages of the monitor are assessed.		
17. KEY WORDS AND DOCUMENT ANALYSIS		
a. DESCRIPTORS	b. IDENTIFIERS/OPEN ENDED TERMS	c. COSATI Field/Group
*Air pollution *Aerosols *Particles *Monitors *Contact potentials *Evaluation		13B 07D
18. DISTRIBUTION STATEMENT  RELEASE TO PUBLIC	19. SECURITY CLASS (This Report) UNCLASSIFIED	21. NO. OF PAGES 80
	20. SECURITY CLASS (This page) UNCLASSIFIED	22. PRICE